



Benthic phosphorus cycling in the northern Benguela upwelling system: excess P supply and altered pelagic nutrient stoichiometry

Peter Kraal¹, Kristin A. Ungerhofer¹, Darci Rush², Gert-Jan Reichart^{1,3}

¹ Royal Netherlands Institute for Sea Research (NIOZ), Department of Ocean Systems, Landsdiep 4, 1797 SZ 't Horntje, The Netherlands

² Royal Netherlands Institute for Sea Research (NIOZ), Department of Microbiology and Marine Biogeochemistry, Landsdiep 4, 1797 SZ 't Horntje, The Netherlands

³ Utrecht University, Faculty of Geosciences, Department of Earth Sciences, Princetonlaan 8a, 3584 CB Utrecht, The Netherlands

Correspondence to: Peter Kraal (peter.kraal@nioz.nl)

Abstract. The northern Benguela upwelling system (NBUS) off Namibia is one of the most productive marine regions globally, with intense biogeochemical cycling and burial of essential elements such as carbon, nitrogen and phosphorus. Element cycling is strongly impacted by temporally and spatially variable degrees of oxygen depletion, both in the water column and the sediment; a perennial oxygen minimum zone (OMZ; minimum $O_2 \sim 50 \mu\text{mol L}^{-1}$) impinges on the slope while the shelf is seasonally oxygen-depleted and even euxinic (i.e. free sulphide in the water column). Areas such as the NBUS are not only significant in regional and global marine element cycles and budgets but can also help predict the impact of globally increasing eutrophication and deoxygenation. Here, we combine biogeochemical water-column and sediment data to explore the (de)coupling of pelagic and benthic nitrogen and phosphorus cycling as function of depositional conditions, particularly deep-water redox. We show major shifts in N:P stoichiometry in deep waters as a result of pelagic nutrient-N (NO_3^- , NH_4^+) loss as N_2 and supply of excess P from the sediment into the bottom water. Notably, benthic P supply contributes strongly to the pelagic N deficit ($\text{PO}_4^{3-} \cdot 16 - \sum(\text{NO}_3^-, \text{NO}_2^-, \text{NH}_4^+)$), which is commonly considered to reflect only the strength of anaerobic N loss. Our results further reflect strong differences in benthic nutrient cycling between depositional environments. The seasonally anoxic shelf hosts organic-rich, strongly reducing sediments with large pools of labile P and high effluxes of DIC and total alkalinity, NH_4^+ , PO_4^{3-} and HS^- . Chemical analysis indicates that a large proportion of the highly reactive sedimentary P pool consists of (i) P supplied in fish debris rather than marine algal biomass and/or (ii) P accumulated intracellularly by sulphide-oxidizing bacteria (SOB). These SOB modulate benthic phosphate and sulphide fluxes, while iron (Fe) redox cycling plays a minor role as the shelf sediments are depleted in reactive ferric iron phases. In contrast to the shelf, slope sediments including those underlying the OMZ are much less organic-rich and show patterns of coupled N and P cycling, the latter coupled to Fe redox cycling. Overall, we show how the distinct environmental conditions on the highly productive and seasonally anoxic shelf drive the decoupling of pelagic and benthic N and P cycles. This results in strongly altered nutrient dynamics and stoichiometry compared to oxygenated marine systems. Such



perturbations are then likely to occur at wider (global) scale in the ocean under conditions of intense oxygen depletion either in the geological past or in the anthropogenic future.

35 1. Introduction

The major nutrients nitrogen (N) and phosphorus (P) are crucial for marine primary productivity and thereby regulate the uptake and (long-term) storage of atmospheric CO₂ in the ocean via the biological pump (Holland, 1978; Ruttenberg, 1993; Falkowski, 1997; Raven and Falkowski, 1999). The bioavailability of N and P for primary producers depends on the balance between supply to and removal from the ocean, which is in turn dependent on ocean oxygenation (i.e. redox conditions). For
40 N, oxygen depletion boosts anaerobic N transformation processes in the water column and sediment that represent a net sink for N through the conversion of inorganic nutrient-N (ammonium, NH₄⁺, and nitrate, NO₃⁻) to inert N₂ (Voss et al., 2013). For P, reducing conditions decrease the sediment P retention capacity and thereby enhance recycling of bioavailable P: oxygen-depleted sediments release a larger fraction of remineralized dissolved phosphate (HPO₄²⁻) to the overlying bottom waters (Ingall and Jahnke, 1994; Slomp et al., 2004; Gächter et al., 1988). The disparate responses of the marine
45 biogeochemical N and P cycles to changes in redox conditions have been linked to marked changes in nutrient availability, stoichiometry and ocean biogeochemistry during past environmental perturbations associated with ocean deoxygenation, such as ocean anoxic events (Jenkyns, 2010; Kuypers et al., 2004; Mort et al., 2007). However, our incomplete understanding of the impact of such perturbations on (de)coupled N and P cycling inhibits accurate reconstruction of ancient ocean biogeochemical feedbacks and the co-evolution of redox conditions and nutrient cycles on Earth (Reinhard et al.,
50 2017; Stüeken et al., 2016). Such feedbacks are also of importance considering the globally increasing extent and intensification of contemporary marine oxygen depletion, which is strongly connected to anthropogenic climate change and eutrophication (Breitburg et al., 2018; Oschlies et al., 2018; Diaz and Rosenberg, 2008; Middelburg and Levin, 2009).

Among marine systems that undergo seasonal, periodic or permanent oxygen depletion and are thus relevant to study redox-dependent marine N-P dynamics, upwelling areas are of great interest. These highly productive ocean regions are
55 biogeochemical hotspots with large faunal stocks and intense organic matter and element fluxes that are of great ecological and economic importance. Prominent upwelling systems are the four major eastern boundary upwelling systems (EBUS), associated with the California, Humboldt, Canary and Benguela current systems (Chavez and Messié, 2009). These four EBUS together represent 1% of ocean area but 5% of global primary productivity and 20% of global fish stocks (Messié and Chavez, 2015). The high organic matter fluxes boost the respiratory oxygen demand, resulting in relatively strong oxygen
60 depletion and even anoxia (i.e. absence of dissolved O₂ for respiration) in intermediate (the so-called oxygen minimum zone, OMZ) and shelf waters of EBUS. Where the oxygen-depleted waters intersect with the seafloor on the slope and shelf, the spatially and temporally variable patterns of oxygen availability in the EBUS (i) modulate living conditions and communities of microbial and higher life and (ii) control the biogeochemical reaction pathways that determine the abundance and fate of the key macronutrients N and P.



65 Through benthic-pelagic coupling, altered benthic biogeochemical functioning can affect pelagic nutrient availability and stoichiometry, particularly in shallow waters such as EBUS shelf environments (Marcus and Boero, 1998; Dale et al., 2017). Because EBUS are directly connected to the open ocean, the element fluxes on the shelf and particularly benthic efflux of essential elements such as P can have large-scale (regional) effects on ocean biogeochemistry (Dale et al., 2017; Giraud et al., 2008; Ruttenberg, 2014b). The open-ocean connection also means that the anthropogenic impact on deoxygenation and

70 water quality (eutrophication) is less than in restricted (coastal) marine systems such as the Baltic Sea (Conley et al., 2011; Meier et al., 2011) and the Black Sea (Kideys, 2002). However, climate change is increasing the extent and intensity of oxygen depletion in (eastern boundary) upwelling systems (Oschlies et al., 2018; Stramma et al., 2008; Bograd et al., 2023). As yet, the (cascading) effects of increased deoxygenation on the ecology and coupled biogeochemical cycles in upwelling systems are poorly understood.

75 Here, we determine the (de)coupling of N and P cycling as function of redox conditions under upwelling conditions in the northern Benguela upwelling system (BUS) off Namibia in the southeast Atlantic Ocean. The BUS is a relatively small EBUS, with a perennial OMZ that occurs between 200–400 meters below the sea surface (mbss) and spatially and temporally strongly variable redox conditions on the shelf. Recent work in the research area has shown extensive N loss from anoxic shelf waters, likely attributable to water-column denitrification (Van Kemenade et al., 2022; Nagel et al., 2013).

80 Redox-dependent N and P biogeochemical cycling in this region results in the off-shelf transport of waters that are characterized by a P excess. This subsequently fuels N fixation in Angolan shelf waters to the north when currents transport the relatively N-depleted waters into the Angolan Gyre (Flohr et al., 2014). In the BUS off Namibia, however, little is known about the benthic P dynamics and recycling as function of depositional conditions and how these processes contribute to the (relative) P excess in the water column. High concentrations of phosphate have been measured in shelf sediments and

85 attributed to P accumulation and release by microbes (*Thiomargarita* sp.), and subsequently linked to modern phosphorite formation (Schulz and Schulz, 2005; Goldammer et al., 2010). Regarding the chemical P pools in the sediment, Küster-Heins et al. performed chemical sequential extractions of slope sediments (~1000 mbss) that indicated that calcium phosphate (Ca-P) in fish debris is an important P burial phase and potentially a source of dissolved P. What remains missing so far, despite these few studies into specific depositional environments, is more integral insight into P burial and

90 regeneration mechanisms as function of variable depositional conditions on the shelf and slope.

We performed sampling and chemical analysis of the water column and sediment over a redox gradient from the anoxic shelf to the oxygenated slope in the northern Benguela upwelling system (BUS) off Namibia (22–25 °S; 100–1500 meters below sea surface, mbss; dissolved-oxygen gradient from 3 to 180 $\mu\text{mol L}^{-1}$, equivalent to ~ 0–50 % saturation). For an integrated picture of N and P cycling, we combine water-column profiles of dissolved nutrients and supporting chemical parameters

95 with chemical analyses of pore-water and bulk sediment composition as well as chemical forms of iron (Fe), P and sulphur (S) in surface sediments (0–40 cm sediment depth). We find that a combination of benthic and pelagic processes result in strong alteration of pelagic N and P concentrations and stoichiometry on the shelf under strongly oxygen-depleted conditions. High rates of P release from labile pools in the uppermost sediment drive an efficient return flux of P to the water

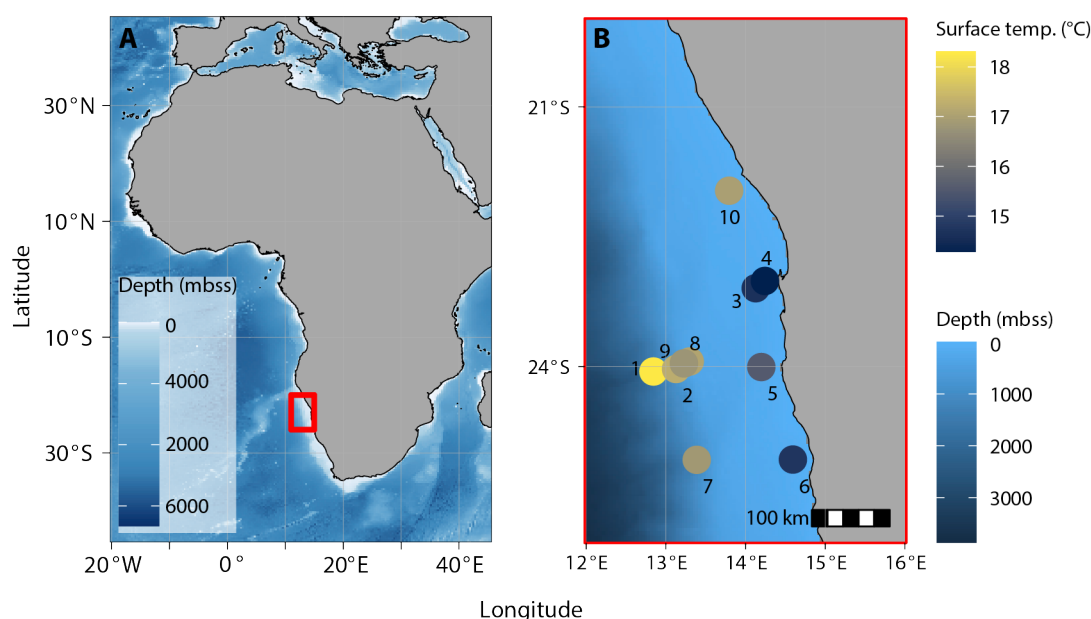


column. In light of the global marine relationships between nutrient stoichiometry, microbial community composition and rates of primary productivity and remineralization (Moore et al., 2013; Moreno and Martiny, 2018; Lenton and Klausmeier, 2007), our results provide important new insight into the impact of extending and intensifying oxygen depletion on ocean biogeochemistry.

2. Materials and Methods

2.1. Research area and sampling stations

Between 1 and 12 February 2019, The FUNAMOX (biogeochemical FUNCTIONING in NAMibian OXYgen-depleted waters) research expedition with RV Pelagia (cruise code 64PE449) was undertaken on the shelf and slope in the northern part of the BUS off the coast of Namibia between 22° and 26° S (Fig. 1). In the research area, shallow waters are characterized by high



productivity

Figure 1: Bathymetric map of eastern Atlantic Ocean with general research area indicated by the red square (a) and bathymetric map of research area with research stations (b). Colour in (b) indicates surface-water (~10 mbss) temperature; low temperatures at shelf stations indicate upwelling of relatively cold deep waters. Bathymetric maps made with ggOceanMaps in Rstudio.

and oxygen depletion as a result of upwelling of high-nutrient and low-oxygen waters from the deep sea (Emeis et al., 2017; Chapman and Shannon, 1987; Shannon et al., 1987; Summerhayes et al., 1995). Upwelling and current patterns result in (i) a perennial OMZ with dissolved O_2 concentrations down to $\sim 50 \mu\text{mol L}^{-1}$ on the slope between $\sim 200 - 400$ mbss, and (ii) seasonal bottom-water anoxia on the shelf (< 100 mbss) with recurring events of water-column anoxia and sedimentary



release of hydrogen sulphide (HS^-) (Nagel et al., 2016; Van Kemenade et al., 2022; Mohrholz et al., 2014; Ohde and Dadou, 2018). The northern BUS (NBUS) is a region with its own distinct seasonality of wind forcing and upwelling (Emeis et al., 2017) with most intense oxygen depletion on the shelf in late austral summer, i.e. January–February (Mohrholz et al., 2008; Brüchert et al., 2006).

During FUNAMOX, water and sediment were sampled at shelf and slope stations between 100 and 1500 mbss, from the anoxic shelf to the oxygenated slope below the perennial OMZ. Physicochemical properties were measured throughout the water column at each station by conductivity-temperature-density (CTD, Seabird SBE 911plus), oxygen (Seabird SBE 43), fluorescence and turbidity (Seabird ECU FLNTU) sensors mounted on a rosette with 24 polypropylene water-sampling bottles (volume 12 L). Discrete water samples were taken by remotely closing sampling bottles at selected depths for subsequent sub-sampling and (on-board) chemical analyses (see below). Surface sediments were collected with a multi-corer (Oktopus GmbH) holding with 10 polycarbonate tubes (10-cm diameter).

2.2. Water-column sampling and analysis

Immediately after the CTD/rosette with sampling bottles was back on deck, the bottles with water samples from selected depths were sub-sampled for a range of dissolved species as detailed in Table 1. First, a 30-mL sample was taken with a polypropylene syringe and filtered over a 0.8/0.2 μm syringe filter (Pall Acropak) that was rinsed three times with sample water. After sampling all bottles, water samples were taken into a laboratory container and sub-sampled for: total alkalinity (TAlk); dissolved inorganic carbon (DIC); soluble reactive P (SRP; here referred to as HPO_4^{2-} , the dominant species at seawater pH of 8.2) and Si (H_4SiO_4); NH_4^+ , NO_2^- and NO_3^- (together termed dissolved inorganic nitrogen, DIN). All these analytes were measured by segmented-flow analysis (QuAatro auto-analyser, AA). Samples for HPO_4^{2-} and Si were acidified to pH ~ 1 .

Table 1: Sampling, treatment and analysis of aqueous samples. Note: sub-samples for HS^- were only taken from pore-water.

Analyte	Preservation	Method	Storage
DIC	15 μL HgCl_2 (no headspace)	On-shore, AA	4 °C
HPO_4^{2-} , Si	10 μL 5 N s.p. HCl mL^{-1}	On-shore, AA	4 °C
NH_4^+ , NO_2^- , NO_3^-	n/a	On-board, AA	n/a
Total alkalinity (TAlk)	15 μL HgCl_2	On-shore, AA	4 °C, gastight bags
Total (dissolved) N, P	n/a	On-shore, digest + AA	-20 °C
Sulphide (HS^-)	10 mmol L^{-1} NaOH , 1% zinc acetate	Manual colorimetry	4 °C

At stations 2 (750 mbss) and 6 (100 mbss), in addition to SRP and DIP measurements, another set of sub-samples was taken at selected depths for analysis of total and total dissolved P and N: one 10-mL sample was directly transferred into a pre-rinsed 15-mL polypropylene centrifuge tube, the second 10-mL sample was filtered over an acid-cleaned 0.2- μm PES filter



into a pre-rinsed 15-mL polypropylene centrifuge tube. At NIOZ, these samples were analysed for total N and P by AA preceded by digestion of (particulate) organic compound using persulfate oxidation and UV irradiation. The difference between total dissolved N and DIN ($\text{NH}_4^+ + \text{NO}_2^- + \text{NO}_3^-$) was assumed to represent dissolved organic N (DON). The difference between total dissolved P and HPO_4^{2-} was assumed to represent dissolved organic P (DOP). The difference between filtered and unfiltered totals represents particulate N and P.

2.3. Sediment sampling and analysis

Immediately after recovery, sediment cores collected with the multi-corer were checked to ensure the sediment surface was intact and that cores were otherwise undisturbed. Several cores were then processed for a suite of analyses.

One core was immediately transported into the dry lab, where replicate O_2 micro-profiles were collected with Unisense OX-50 (50- μm tip) glass micro-electrodes operated with a micromanipulator and connected to a Unisense PA2000 picoamperometer. Resolution of measurement was 250-1000 μm , decreasing with sediment depth. Profiles were aborted when O_2 reached 0. For replicate measurements, the micro-electrode was moved to a new, flat and undisturbed location on the sediment surface. The O_2 readings are reported as % air saturation at ambient bottom-water temperature; O_2 profiles and information on the temperature calibration at 100% air saturation can be found in the Supplementary Information. Diffusive O_2 uptake by the sediment at each station was calculated from the dissolved O_2 gradient in the diffusive boundary layer. Stations with strongly oxygen-depleted bottom water (3, 4, 5, 6, 10) were omitted.

A second core was placed on a hydraulic core slicer in a temperature-controlled container set to bottom-water temperature and the core was sectioned into intervals of 0.5–4 cm, the resolution decreasing with depth. A sub-sample of each sediment interval was transferred into a pre-weighed 20-mL plastic container that was stored at -20°C until further processing. The remaining sediment from each interval was transferred into a geochemical sampling bag and stored frozen. Back in the NIOZ laboratory on shore, the 20-mL containers with frozen wet sediment were weighed, freeze-dried and then weighed again; the mass loss was used to calculate the gravimetric water content, from which the porosity was subsequently calculated (Burdige, 2006). In addition, the water content was used to correct sample masses for various solid-phase analyses for the contribution of sea salt from seawater after freeze-drying, which was significant (up to ~50% of dry sample mass) especially in top samples with high porosity.

A third core was immediately transferred into a N_2 -purged glove bag in a temperature-controlled container set at bottom-water temperature. A bottom-water sample was taken about 10 cm above the sediment surface with a 20-mL syringe; this sample was processed together with the pore-water samples. Subsequently, the sediment was sliced at the same vertical resolution as the core sectioned for porosity and ^{210}Pb . Sediment slices were transferred into centrifuge tubes that were centrifuged for 30 min at 4000 rpm and transferred into a second N_2 -purged glove bag, where the pore-water was decanted into acid-cleaned 20-mL polypropylene syringes and filtered using acid-cleaned 0.2- μm PES syringe filters. The filtered pore-water was subsampled for analysis of dissolved species like water-column samples, as detailed in Table 1.



With principles outlined in Burdige and Komada (2011) and adapted by Jilbert et al. (2020), we used the measured pore-water NH_4^+ profile to calculate the expected dissolved HPO_4^{2-} profile that would result from breakdown of algal organic matter with Redfield N/P stoichiometry (16) (Redfield, 1958) and simple accumulation of the released HPO_4^{2-} in the pore-water:

$$180 \quad \frac{d\Delta\text{NH}_4^+}{d\Delta\text{H}_2\text{PO}_4^{2-}} = -r_{\text{N:P}} \times \frac{D_{\text{H}_2\text{PO}_4^{2-}}}{D_{\text{NH}_4^+}}, \quad (1)$$

where $d\Delta[\text{species}]$ represents pore-water concentration gradient over depth, $r_{\text{C:P}}$ represents expected molar ratio of N:P in remineralized organic matter (assumed to be 16), and D_{species} represents sediment diffusion coefficients of HPO_4^{2-} and NH_4^+ , calculated at in situ temperature, salinity and pressure in R package marelac and corrected for sediment porosity.

The wet sediment residue was stored under N_2 in gas-tight aluminium-laminate bags at -20°C to minimize alteration of the original sediment chemistry. At NIOZ, the frozen wet sediment residue was allowed to thaw in a N_2 -purged glove bag. A well-mixed sub-sample of the wet sediment was taken, weighed and gravimetric water content was determined from mass loss after freeze-drying. The freeze-dried material was ground and used for measurement of (i) total organic carbon (TOC) and nitrogen (N), and (ii) total elements. For TOC and TN, a sub-sample of the freeze-dried and ground sediment was weighed into a tin cup and subsequently decalcified by placing it in a desiccator containing an open beaker of fuming HCl for 12 hours and subsequently adding two aliquots of $30\ \mu\text{L}$ $2\ \text{M}$ HCl to each sample before re-drying them in an oven at 60°C for one hour (modified protocol of Needoba et al. (2007)). The TOC and N content in the carbonate-free sediment was measured with a Thermo-Interscience Flash EA 1112 CN analyser. Total major and minor elements (Al, Ca, Cd, Fe, Mn, Mo, P, S, V) were measured in acid digests of the sediment with a Thermo Scientific Element 2 high-resolution ICP-MS. For acid digestion, about 100–125 mg of the freeze-dried and homogenized sediment was digested in a closed Teflon vessel on a hot block in a mixture of 2.5 mL HF, 1 mL HNO_3 , 1.5 mL HClO_4 and 1 mL HCl at 90°C for 12 hours. Subsequently, the acid mixture was evaporated to near dryness at 190°C , after which the residue was re-dissolved in 20 mL of $1\ \text{M}$ HNO_3 at 110°C overnight.

From the thawed wet sediment in the N_2 -purged glove bag at NIOZ, three sub-samples were taken for sequential chemical extraction of Fe, P and S (Table 2). A modified protocol based on Poulton and Canfield (2005) and Claff et al. (2010) as presented in Kraal et al. (2017) was used to extract highly reactive Fe, which has been defined by Poulton and Canfield (2005) as the combined Fe pools that are reactive towards or have reacted with dissolved sulphide. Iron concentrations in the extracts were determined with the 1,10-phenanthroline method (Apha, 2005). In the $1\ \text{M}$ HCl extracts (i.e. labile Fe), Fe(II) and total Fe were determined by measuring Fe before and after adding the reducing agent hydroxylamine, respectively; Fe(III) was then calculated by difference.

For P, total P was fractionated using the protocol of Ruttenberg (1992). Phosphorus concentrations in the extracts were determined with the molybdate-blue method (Apha, 2005). For the dithionite extracts, this was done following the sample pretreatment detailed in Anschutz et al. (2005) to overcome issues with the matrix.



210 **Table 2: Sequential extraction protocols for highly reactive iron, total phosphorus and reduced inorganic sulphur.**

Extraction	Target phase	Name
<i>Sedimentary iron pools</i>		
1 mol L ⁻¹ HCl (pH 0, 1 h)	Labile, poorly ordered and pH-sensitive ferric (e.g. ferrihydrite) and ferrous (e.g. iron monosulphide, siderite) iron minerals	HCl-Fe(II), HCl-Fe(III)
0.35 mol L ⁻¹ acetic acid/0.2 mol L ⁻¹ Na ₃ -citrate/50 g L ⁻¹ Na dithionite (buffered pH 4.8, 4 h)	Crystalline oxide minerals (goethite, hematite)	CDB-Fe; crystalline Fe ^b
0.17 mol L ⁻¹ NH ₄ oxalate/0.2 mol L ⁻¹ oxalic acid (buffered pH 3.2, 6 h)	Recalcitrant oxide minerals (magnetite) ^a	Oxalate-Fe; crystalline Fe ^b
65% HNO ₃ (pH < 0, 2 h)	Pyrite	HNO ₃ -Fe
<i>Sedimentary phosphorus pools</i>		
1 M MgCl ₂ (brought to pH 8 with NaOH, 0.5 h)	Exchangeable P	Ex-P
0.3 mol L ⁻¹ Na ₃ citrate/1 mol L ⁻¹ NaHCO ₃ /25 g L ⁻¹ Na dithionite (buffered pH 7.6, 8 h) ^c	P bound to easily reducible Fe(III) (oxyhydr)oxides; P in vivianite ^b (Fe(II) ₃ (PO ₄) ₂ ·8H ₂ O)	CDB-P
1 mol L ⁻¹ Na acetate buffered to pH 4 with CH ₃ COOH (6 h) ^c	Carbonate fluorapatite, hydroxyapatite	Ca-P
1 mol L ⁻¹ HCl (pH 0, 24 h)	P in detrital minerals	Det-P
Ashing residue at 550 °C (2 h), followed by 1 mol L ⁻¹ HCl (24 h)	P in organic matter	Org-P
<i>Sedimentary reduced inorganic sulfur pools</i>		
6 mol L ⁻¹ HCl (24 h)	Acid-volatile sulfur (AVS); iron monosulphide	AVS
Methanol (16 h), followed by acetone rinse (20 min)	Elemental sulfur	ES
500 g L ⁻¹ chromous chloride in 32% HCl (48 h)	Chromium-reducible sulfur (CRS): pyrite and marcasite	CRS

^a Due to likely partial dissolution of magnetite in 1M HCl (Poulton and Canfield, 2005) and the acetic acid–citrate–dithionite solution (Claff et al., 2010), this likely only represents the most recalcitrant magnetite.

^b In light of the above uncertainty, CDB-Fe and oxalate-Fe are collectively referred to as crystalline Fe(III).

215 Reduced inorganic sulphur (RIS) pools (i.e. metal monosulphides, elemental sulphur, pyrite) were extracted following the protocol detailed in Kraal et al. (2013) based on the passive sulphide extraction method presented in Burton et al. (2008).



The AVS and CRS were quantified by iodometric titration (Apha, 2005), the ES was quantified using the cyanolysis method detailed in Bartlett and Skoog (1954).

2.4. Benthic flux measurements by on-deck, whole-core incubations

220 At selected stations, three multi-core tubes were equipped with Presens (GmbH) oxygen spots and, after core recovery from the seafloor, capped with custom-made gas-tight lids with two ports and a stir motor. The core tubes contained ~25 cm sediment and 35 cm overlying water. One port was connected to a 10-L carboy with water from the deepest CTD/rosette bottle collected at the station, usually 5-10 m above the seafloor. The second port was used as sampling port, through which 20-mL samples of the overlying water were taken with an acid-cleaned, 30-mL polypropylene syringe at different time
225 intervals. The sampled water was replenished through the port connected to the container with bottom water. The overlying water was continuously stirred and O₂ was measured every 5 min using a Presens OXY-4 setup with fiber optic cables and sensor spots, operated with the Presens Measurement Studio 2 software.

The water samples were immediately filtered using 0.2-μm acid-cleaned PES syringe filters and sub-sampled for: DIC, TAlk, major and minor elements (metals), NH₄⁺, NO₂⁻, NO₃⁻, HPO₄²⁻, Si, as described in Table 1. Concentration changes of
230 analytes in the overlying water in combination with elapsed time, sediment area and volume of overlying water were used to calculate benthic fluxes:

$$F_i = \Delta C / \Delta t \times V / A, \quad (2)$$

where F_i is the measured flux of analyte i (mmol m⁻² d⁻¹), $\Delta C / \Delta t$ is the rate of concentration change (μmol L⁻¹ d⁻¹) measured in the overlying water, V is the volume of overlying water (dm³), and A is the area of sediment surface in the core (dm²).

235 Measured whole-core-incubation fluxes were compared to diffusive fluxes calculated using pore-water and bottom-water profiles for selected elements with Fick's First Law:

$$J_i = -\varphi \times D_{sed} \times \delta C / \delta z, \quad (3)$$

where J_i is the calculated diffusive flux of the element i (mmol m⁻² d⁻¹); φ is the sediment porosity (cm³ cm⁻³) calculated from gravimetric water content; D_{sed} is the sediment diffusion coefficient for the analyte at ambient temperature (s cm⁻²), pressure and salinity calculated using the *R* package *marelac* corrected for sediment tortuosity (Burdige, 2006); $\delta C / \delta z$ is the
240 concentration gradient across the sediment-water interface (mmol cm⁻⁴). The latter was calculated from the analyte's concentration in the bottom water (overlying water) and first pore-water sample (0.5 cm sediment depth).

3. Results

A summary of key sediment and bottom-water properties can be found in Table 3. The investigated stations were grouped as
245 shelf, OMZ and slope stations. Shelf stations (6, 10, 5, 4, 3) had water depths of around 100 m, deep waters with relatively high temperatures of 12–13 °C and low oxygen concentrations (3–10 μmol L⁻¹), and surface sediment (0–2 cm) that were



strongly enriched in TOC (10–20 wt.%). The OMZ stations (8, 9) were located at intermediate depths of 300–400 mbss with colder (8 °C) and better oxygenated (65 $\mu\text{mol L}^{-1}$) deep waters compared to the shelf, while TOC contents (3 wt.%) in surface sediment that were the lowest of the investigated transect. The slope stations (1, 2, 7) between 750 and 1500 mbss were characterized by lowest deep-water temperatures (3–5 °C), relatively high oxygen concentrations (100–180 $\mu\text{mol L}^{-1}$) and organic-rich surface sediment (4–7 wt.% TOC).

Table 3: Overview of selected key parameters for the investigated stations, grouped as shelf, OMZ and slope stations. Note that not all parameters were determined at all stations, missing data indicated as n.d. (not determined). TOC represents surface sediment (top 2 cm), standard deviation between parentheses (TOC not determined for stations 5 and 9).

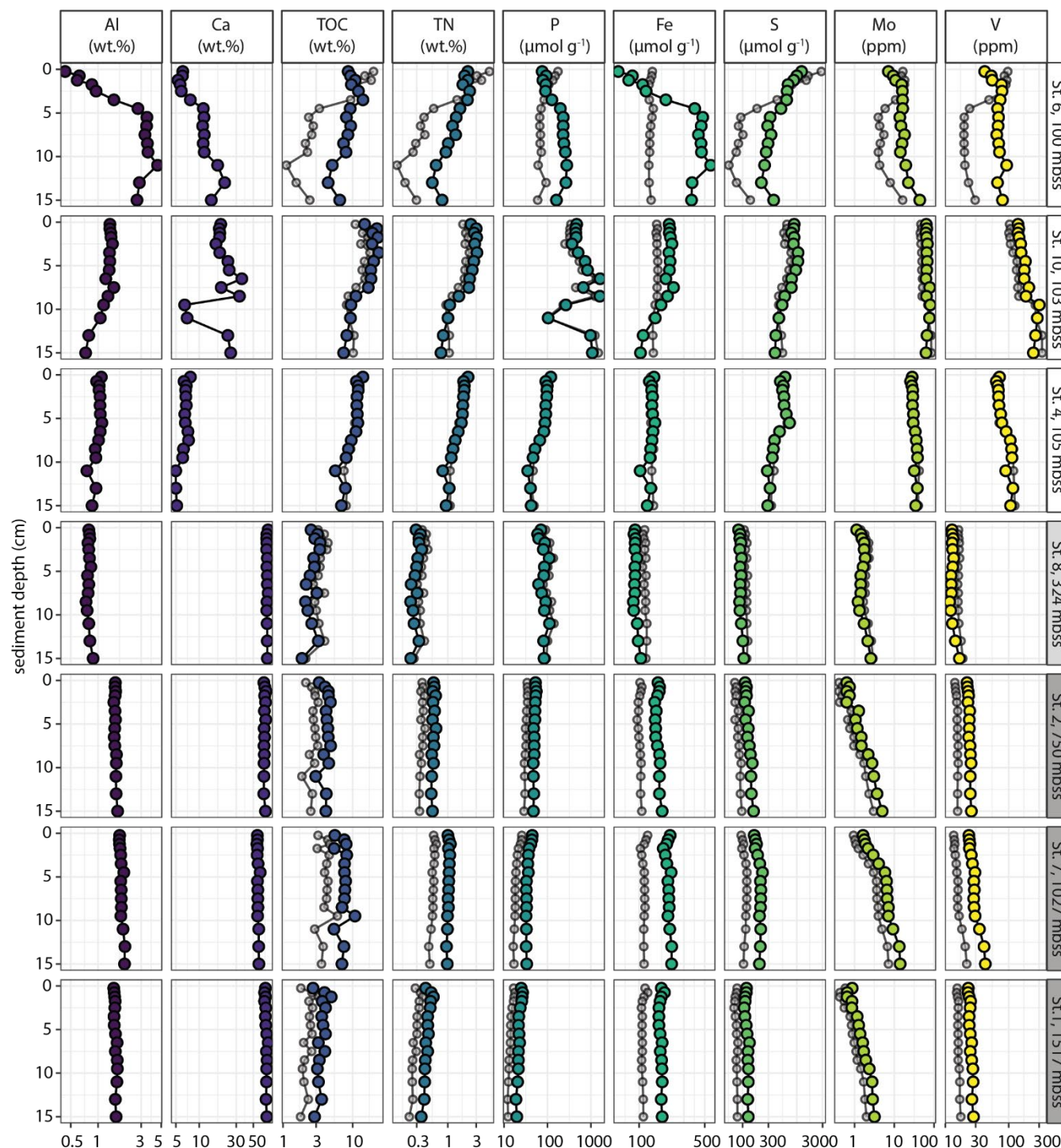
Station	Lat (S)	Long (E)	Depth (mbss)	Group	Temp (°C)	BWO ($\mu\text{mol L}^{-1}$)	BWO (% sat.)	O ₂ pen. (mm)	TOC (wt.%)
6	25.072	14.596	100	Shelf	12.3	2.9	1	0.25	9.6 (0.9)
10	21.968	13.793	103	Shelf	13.5	3.0	1	0.25	19.8 (3.7)
5	24.005	14.198	102	Shelf	12.8	5.9	2	0.5	-
4	23.011	14.244	105	Shelf	13.1	9.7	4	0	12.3 (1.2)
3	23.096	14.128	136	Shelf	12.3	18.2	7	0	12.3 (0.3)
8	23.939	13.299	324	OMZ	8.4	65.3	22	1.5	3.0 (0.4)
9	23.962	13.226	407	OMZ	8.4	64.8	22	1.25	-
2	24.026	13.126	750	Slope	5.3	105.9	34	4	4.1 (0.6)
7	25.075	13.389	1027	Slope	3.8	146.2	45	3	6.7 (1.4)
1	24.056	12.843	1517	Slope	3.3	178.7	54	> 2 ^a	3.8 (0.9)

^a Incomplete profile; zero O₂ not reached at 2 mm sediment depth

3.1. Sediment chemistry

Bulk solid-phase elemental profiles showed contrasting sediment chemistry between the shelf and slope sites (Fig. 2). The CaCO₃ content was relatively low (12 ± 8 wt.%, range 0–40 wt.%) in sediments on the shelf, while TOC was strongly enriched (mean 12 ± 5 wt.%) with a maximum of 26 wt.%. The highest CaCO₃ and TOC contents were measured in sediment at station 10, which also stood out because of the high and variable P content of up to 1500 $\mu\text{mol g}^{-1}$ (4.6 wt.%), correlating with Ca content. Concentrations of Fe, P, S, Mo and V were (much) higher in shelf sediments than slope sediments, where the CaCO₃ content was high (69 ± 7 wt.%) and TOC was lower than on the shelf but still high: 5 ± 2 wt.% (range 3–11 wt.%). Solid-phase manganese concentrations were very low at all stations, with a maximum of 6 $\mu\text{mol g}^{-1}$ (data not shown).

The shelf stations showed downward increasing TOC/N, most notably at stations 6 and 10 where values increased from 4–7 to 10–11. The molar TOC/N ratios revealed no down-core trend but considerable scatter in slope and OMZ sediment with



270 **Figure 2: Sediment profiles of key solid-phase chemical parameters plotted against sediment depth. Al-normalized profiles are shown in semi-transparent grey.**

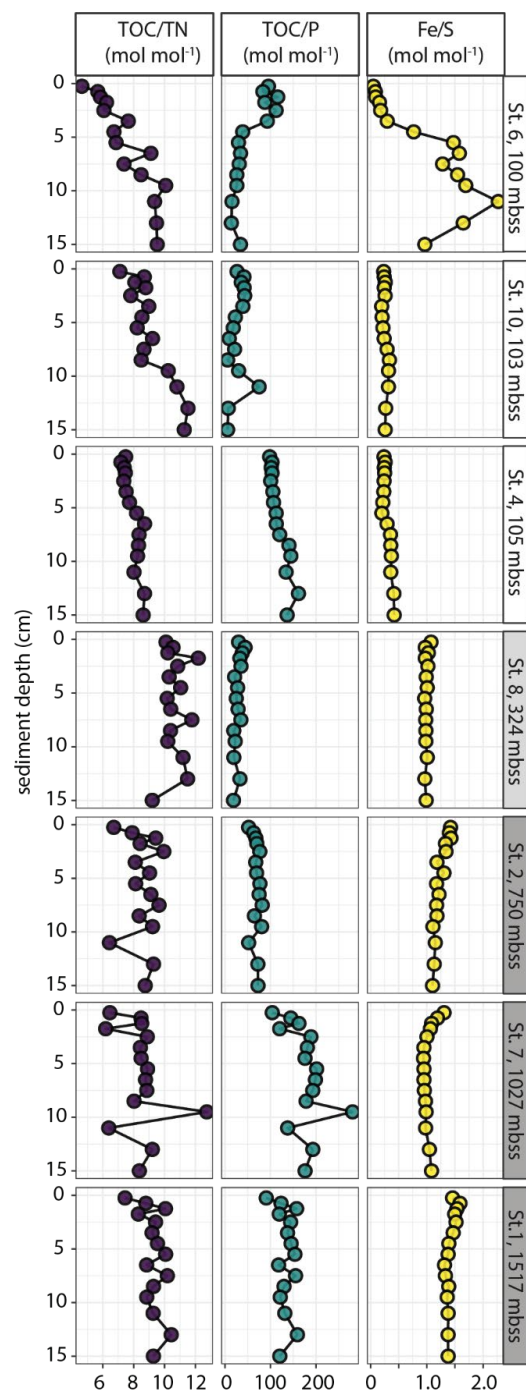


Figure 3: Molar ratios of sedimentary TOC/N, TOC/P and Fe/S plotted against sediment depth for selected stations.



275 values of 8 – 10 and 10 – 12, respectively (Fig. 3). The molar TOC/P ratio showed large variability between stations across
the different depositional environments with values < 100 on the shelf, in the OMZ and on the upper slope (station 2), while
values of 100–200 were observed at the deepest slope stations 7 and 1. The lowest values were measured in sediment at
station 10: average 28 ± 19 , range 6 – 78). The molar Fe/S ratio was relatively constant down-core at most stations and
showed an overall increase from the shelf (< 0.5) to the slope (1–1.5). Again, Station 10 stood out, this time with a strong
280 down-core increase in $\text{Fe}_{\text{tot}}/\text{S}_{\text{tot}}$ from <0.1 to a maximum of 2.3 at depth.

The sedimentary Fe pool was dominated by poorly reactive and unreactive Fe (PR-Fe in Fig. 4A), which made up 73 ± 11 %
of total solid-phase Fe. Only at sediment depth > 5 cm at station 7 was reactive Fe quantitatively more important than PR-Fe.
The major reactive Fe pools were HCl-Fe(II), CBD-Fe and HNO_3 -Fe that all accounted for 5–20% of Fe at the selected
stations. At Station 4, a small but persistent pool of HCl-Fe(III) was detected.

285 The solid-phase S pool consisted predominantly of organic S (Fig. 4B), which accounted for 61 ± 17 % of total S. The
deeper sediment at station 7, with relatively high reactive Fe, contained relatively large pools of AVS and particularly CRS,
together making up more than 80 % of the total S pool. In sediments of the slope stations, reduced inorganic S (RIS) was
dominated by AVS and CRS, while AVS and elemental sulphur (ES) made up the RIS pool in sediment of the shelf stations,
where CRS was largely absent.

290 The deepest slope station (2; 750 mbss selected for sequential P extraction showed roughly equally sized pools of Fe-
associated, Ca-associated, detrital and organic P, with only minor exchangeable P (Fig. 4C). The sedimentary P pool at slope
station 7 showed a similar P sediment chemistry, with the difference that detrital P was nearly absent. Shelf station 4 showed
concentrations and composition of P pools similar to station 7, but with a large exchangeable P pool in the surface sediment
< 5 cm depth. Shelf stations 6 and 10 showed markedly different sediment P chemistry: total P contents were much higher
295 (values up to $1500 \mu\text{mol g}^{-1}$ rather than 50–150 $\mu\text{mol g}^{-1}$ as found at the other stations, particularly at station 10, and P was
present predominantly as Ca-associated P with minor contributions of exchangeable and/or Fe-associated P. Note that
organic P was not determined for station 10 because of analytical issues; however, mass balance (i.e. total P from sediment
digest compared to cumulative P from SEDEX extraction steps) indicated that this was a minor P pool.

3.2. Pore-water chemistry

300 Micro-profiles of dissolved O_2 around the sediment-water interface showed an increase in oxygen penetration from < 1 mm
at shelf stations to 1.25–4 mm on the slope (Table 3). Pore-water profiles showed the distinct chemistry of shelf stations
compared to OMZ and slope stations (Fig. 5). All DIC profiles showed down-core increases, with much higher
concentrations on the shelf stations (up to 15 mmol L^{-1}) compared to the slope (up to 2.5 mmol L^{-1}). Similarly, pore-water
 NH_4^+ concentrations reached much higher concentration at depth in the sediment on the shelf (up to 2 mmol L^{-1}) than on the
305 slope (up to $60 \mu\text{mol L}^{-1}$). Dissolved nitrate and nitrite concentrations were about an order of magnitude lower than NH_4^+ (up
to 80 and $7 \mu\text{mol L}^{-1}$, respectively), with marked peaks above seawater concentrations at depth in the sediment at the shelf

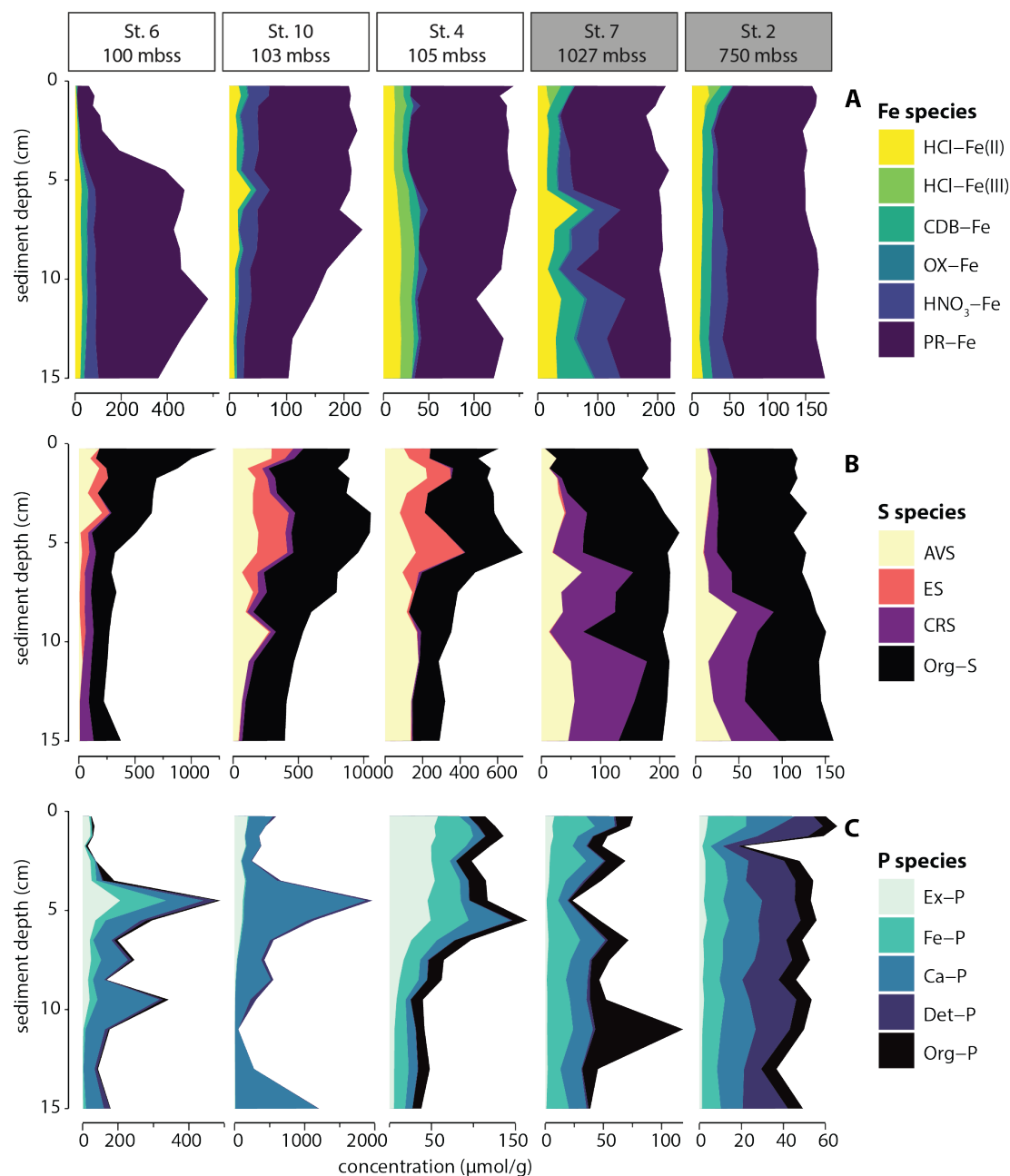
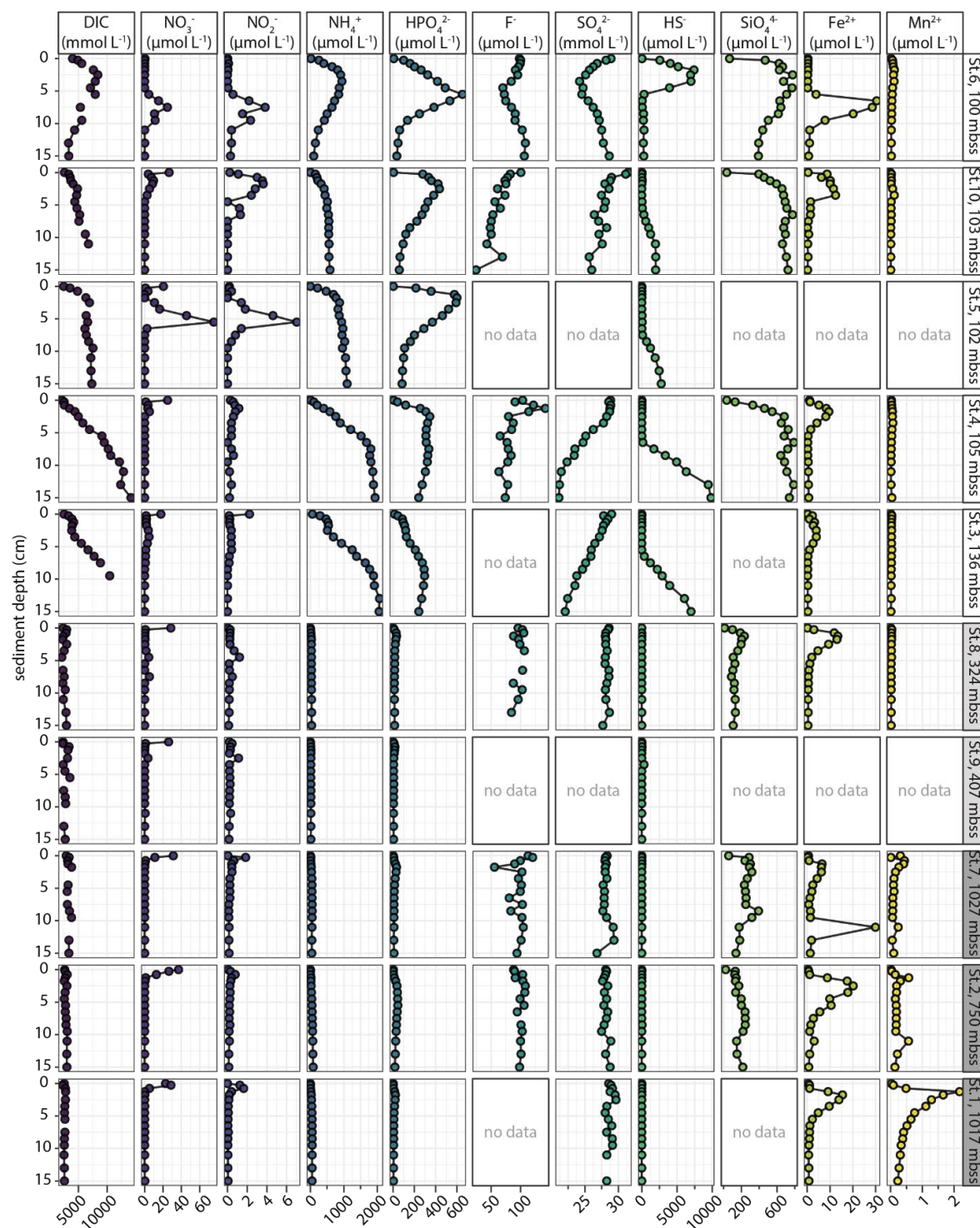


Figure 4: Solid-phase sedimentary iron (a), sulphur (b) and phosphorus (c) pools plotted against sediment depth for selected stations.

stations, particularly stations 5, 6 and 10. Dissolved HPO_4^{2-} showed maxima of 100 and 700 $\mu\text{mol L}^{-1}$ on the shelf and slope, respectively, while dissolved SiO_4^{4-} increased downcore to 800 $\mu\text{mol L}^{-1}$ on the shelf and 400 $\mu\text{mol L}^{-1}$ on the slope. The



315 Figure 5: Key pore-water species plotted against sediment depth.



shelf stations showed down-core decreases in pore-water F^- concentrations (up to 75%; F^- from ~ 100 to $25 \mu\text{mol L}^{-1}$), while dissolved F^- was more stable in slope sediments ($< 10\%$ down-core decrease). Dissolved sulphide (HS^-) was absent or very low in the pore-water at slope stations, where dissolved SO_4^{2-} concentrations were stable at $\sim 28 \text{ mmol L}^{-1}$. By contrast, HS^- concentrations up to 10 mmol L^{-1} accumulated at depth in the shelf sediment, with associated decreases in dissolved SO_4^{2-} . Dissolved Fe and Mn concentrations were very low, up to 30 and $2.5 \mu\text{mol L}^{-1}$, respectively. Dissolved Fe and Mn showed a pattern of sub-surface peaks that increased in magnitude with increasing station water depth, and Fe additionally showed marked enrichments at depth in the sediment of shelf stations, coinciding with NO_3^- peaks. Of the shelf stations, station 6

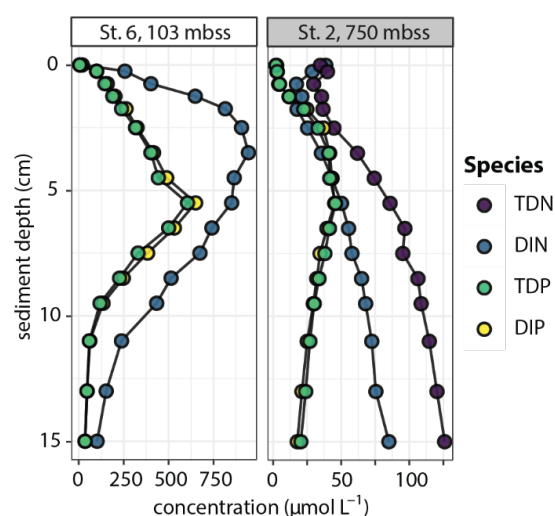


Figure 6: Depth profiles of total dissolved nitrogen (TDN), dissolved inorganic nitrogen (DIN), total dissolved phosphorus (TDP) and dissolved inorganic phosphorus (DIP) in pore-waters at stations 2 and 6, plotted against sediment depth. TDN for station 6 was not determined.

stood out as the only station where pore-water peaks in NH_4^+ , HPO_4^{2-} , HS^- and SiO_4^{4-} occurred in the top sediment rather than at depth.

Analysis of total dissolved N and P in addition to DIN and HPO_4^{2-} at stations 2 and 6 allowed the estimation of pore-water DON and DOP pools (Fig. 6). Total dissolved N and thus the DON pool was only quantified in pore-water from station 2, where it represented a significant dissolved N pool: $10\text{--}45 \mu\text{mol L}^{-1}$, $\sim 25\text{--}50\%$ of total dissolved N. Dissolved organic P was determined in station 2 and 6 pore-waters and was a much smaller pool than DON, both in absolute and relative terms. We first note that DOP calculated as total dissolved P minus P often resulted in negative numbers, indicating the absence of a significant DOP pool. This applied to most measured samples from station 6, where total dissolved P and HPO_4^{2-} concentrations were high, making a calculation by difference of a small P pool challenging. Where calculated DOP values



were positive (mostly station 2 samples where P concentrations were relatively low), DOP ranged between 0.3 and 3.5 $\mu\text{mol L}^{-1}$, accounting for 1–10 % of total dissolved P.

340 Finally, we compared measured HPO_4^{2-} profiles to calculated ‘expected’ HPO_4^{2-} profiles based on DIN and DIP release from organic matter breakdown with Redfield stoichiometry ($\text{N/P} = 16 \text{ mol mol}^{-1}$; see equation 1 in section 2.3). The measured HPO_4^{2-} accumulation strongly exceeded the calculated expected HPO_4^{2-} concentration in the top 5–15 cm of the sediment at all stations except Station 3 (Fig. 7). At greater depth, measured HPO_4^{2-} profiles show a sharp decline, generally to values below expected values. Notable exceptions are the OMZ stations, where measured HPO_4^{2-} were low (5–15 $\mu\text{mol L}^{-1}$) but

345 consistently higher than calculated values.

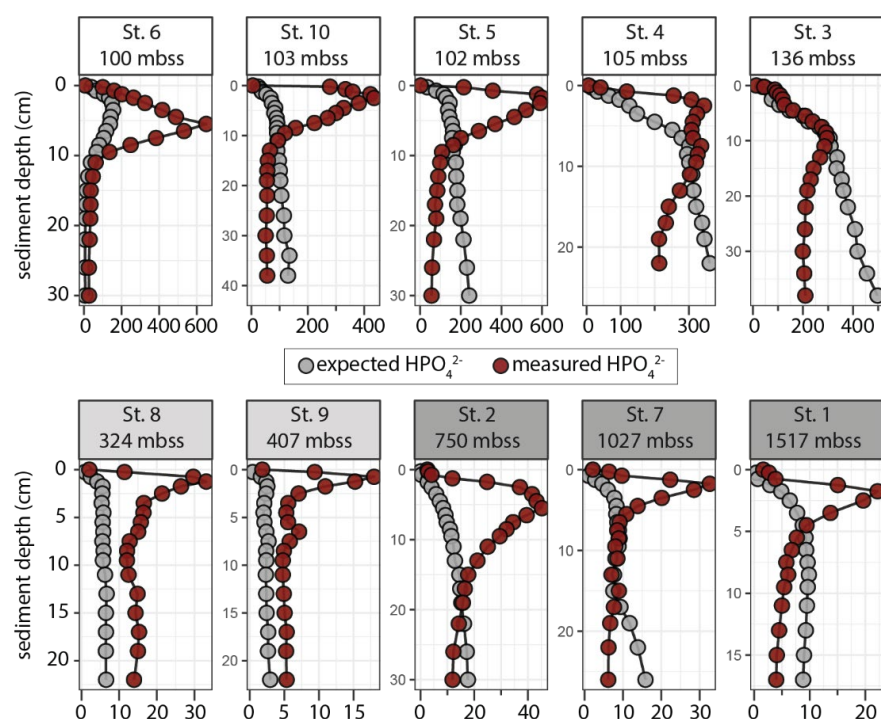


Figure 7: Measured and ‘expected’ dissolved phosphate profiles plotted against sediment depth. The calculated profiles are based on assumed release of NH_4^+ and HPO_4^{2-} from degradation of marine algal organic matter with Redfield stoichiometry ($\text{N/P} = 16$).

350

3.3. Benthic fluxes and bottom-water chemistry

Estimated benthic diffusive fluxes for O_2 (from micro-profiling) and key species (from discrete pore-water samples) show a shelf-to-slope transition from sulphate reduction to oxic respiration as the dominant OM degradation process (Fig. 8, left panels). The DIC scaled with oxygen and sulphate consumption rates, respectively, on the shelf (9–25 $\text{mmol m}^{-2} \text{ d}^{-1}$) and

355 slope (–2–8 $\text{mmol m}^{-2} \text{ d}^{-1}$). The calculated diffusive fluxes of NH_4^+ and HPO_4^{2-} were all positive, up to 11 and 4 $\text{mmol m}^{-2} \text{ d}^{-1}$.

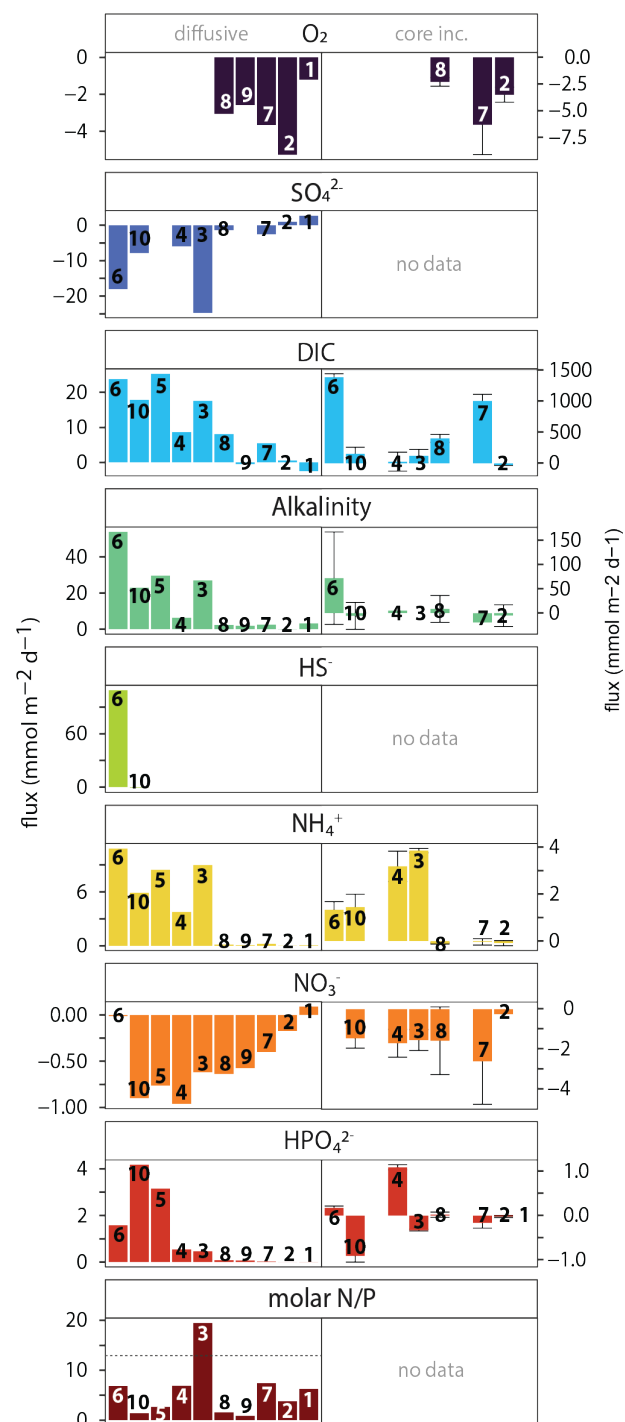


Figure 8: Benthic fluxes for key geochemical species: (left) calculated fluxes using concentration gradient in the diffusive boundary layer (O₂) or the gradient between bottom water and uppermost pore-water sample at 0.25 cm depth (all other species); (right) measured benthic fluxes calculated from changes in bottom-water chemistry during whole-core incubations.



360

¹, respectively, suggesting efflux of these nutrients from the sediment into the overlying water at all stations, with relatively high values on the shelf. A small flux of NO_3^- into the sediment of up to $-1 \text{ mmol m}^{-2} \text{ d}^{-1}$ was calculated for all stations except at station 1 where a small efflux from the sediment ($0.1 \text{ mmol m}^{-2} \text{ d}^{-1}$) was calculated. The molar N/P ratio of the benthic efflux was generally well below the Redfield N/P ratio of 16 (Redfield C:N:P $\approx 106:16:1$), ranging between 1 – 7 mol mol⁻¹. Only at station 3 on the shelf, the benthic flux N/P ratio was close to Redfield (19 mol mol⁻¹). Stoichiometry further showed that the ratio of diffusive DIC and NH_4^+ fluxes (~ 3) was relatively low compared to Redfield (~ 6.5). Lastly, station 6 showed a strong efflux of HS^- from the sediment into the overlying water ($\sim 100 \text{ mmol m}^{-2} \text{ d}^{-1}$), in line with the steep increase in dissolved HS^- in the uppermost sediment (Fig. 6). Only at this station, the diffusive TALK flux ($50 \text{ mmol m}^{-2} \text{ d}^{-1}$) was much larger than the DIC flux ($24 \text{ mmol m}^{-2} \text{ d}^{-1}$).

370 The measured benthic exchange rates generally showed much higher variability than the calculated diffusive fluxes (Fig. 8, right panels). The calculated and measured oxygen consumption rates were similar, ranging between 2 and 6 $\text{mmol m}^{-2} \text{ d}^{-1}$, with somewhat higher values obtained from O_2 consumption in the core incubations. There was, however, a marked difference between the calculated and measured DIC fluxes with highly variable measured DIC fluxes that were particularly high for stations 6 and 7 ($100 - 1500 \text{ mmol m}^{-2} \text{ d}^{-1}$). The accompanying TALK fluxes were about an order of magnitude lower. The measured NH_4^+ and NO_3^- were of similar magnitude as the calculated diffusive fluxes, with relatively low measured fluxes for NH_4^+ . The trends were similar: NO_3^- uptake into the sediment at all stations and NH_4^+ efflux concentrated on the shelf where bottom waters were depleted of oxygen. In contrast to calculated diffusive fluxes, the measured HPO_4^{2-} fluxes did not show a trend from high to low fluxes from the shelf to the slope, but rather strong variation between stations, with negative (uptake) and positive (efflux) fluxes measured on the shelf.

380

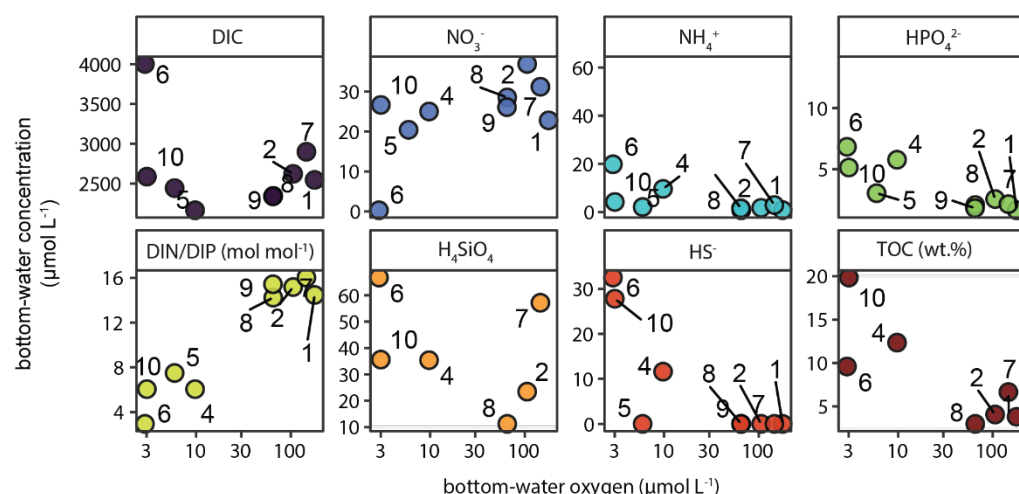


Figure 9: Key chemical parameters in bottom water (i.e. overlying water in sediment cores collected with the multi-corer) as function of bottom-water oxygen (i.e. deepest CTD/rosette measurement, $\sim 5 \text{ m}$ above the seafloor). Unit is $\mu\text{mol L}^{-1}$ unless indicated otherwise. TOC (wt.%) is the average TOC content in the top 2 cm of the sediment at each station.

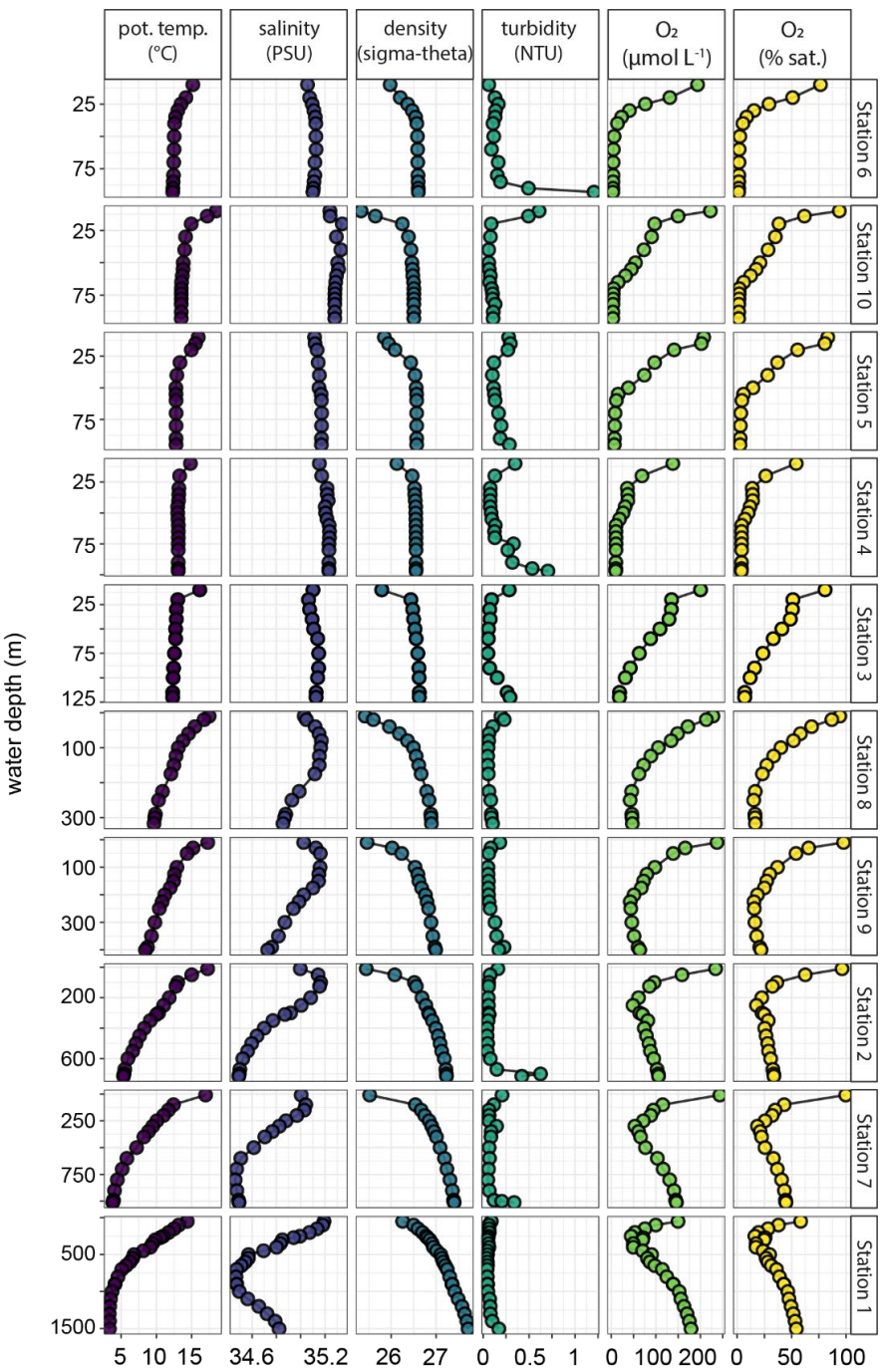
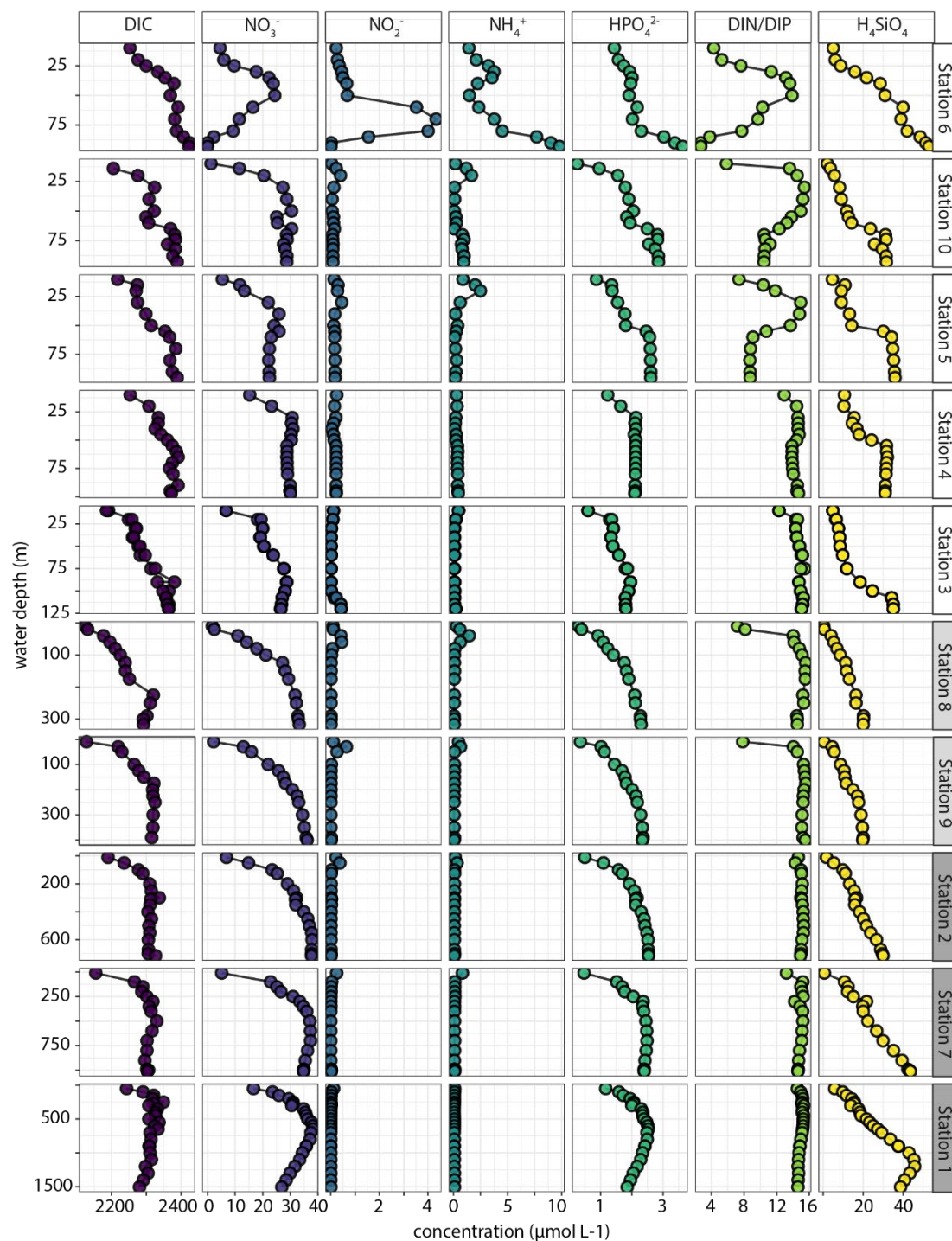


Figure 10: Profiles of key physical and chemical water-column properties plotted against water depth. Stations are in order of increasing water depth.



390 **Figure 11: Water-column C, N, P and Si depth profiles plotted against water depth at the investigated stations. The only derived variable is the total dissolved inorganic N:inorganic P ratio (DIN/DIP). Stations are ordered based on water depth. All species in $\mu\text{mol L}^{-1}$ except DIN/DIP in mol mol^{-1} .**



In addition to pore-water analysis, the bottom water overlying the sediment collected with the multi-corer was sampled and analysed. The results showed that with decreasing O_2 (i.e. moving from the slope up to the oxygen-depleted shelf), NO_3^- decreased while NO_2^- , NH_4^+ , HPO_4^{2-} and SiO_4^{4-} increased (Fig. 9). The opposite trends in bottom-water NO_3^- and HPO_4^{2-} resulted in a marked decline of the DIN:DIP ratio with decreasing oxygen, from near-Redfield (16) to as low as 3. Moreover, accumulation of dissolved HS^- was detected in the bottom water at the stations experiencing strong bottom-water oxygen depletion (Station 4, 6, 10). For context, Fig. 9 also shows the strong increasing trend in surface-sediment TOC content from the slope to the shelf in the bottom left panel.

3.4. Physical and chemical water-column properties

The deepest water samples taken with the CTD/rosette (~5 m above seafloor) across the depth transect from shelf to slope showed oxygen concentrations between 3 and 179 $\mu\text{mol L}^{-1}$, equivalent to 1–54 % saturation calculated using in-situ salinity and temperature (Fig. 10).

Water-column profiles of key physical and chemical parameters (Fig. 10) showed oxygen-depleted waters in the bottom 25–50 m of the water column on the shelf, except at station 3. The OMZ stations were located where the core of the perennial OMZ intersected the slope, with oxygen concentrations around the threshold for hypoxic conditions (63 $\mu\text{mol L}^{-1}$). Below the OMZ, dissolved oxygen increased to 179 $\mu\text{mol L}^{-1}$ (54 % saturation) at 1500 mbss. Salinity profiles indicated the presence of a distinct, low-salinity water mass between 500–1000 mbss. The turbidity profiles showed increased turbidity in bottom waters, most prominently at stations 2, 4 and 6.

The water-column profiles of dissolved carbon and nutrients (DIC, NH_4^+ , NO_2^- , NO_3^- , HPO_4^{2-} , SiO_4^{4-} ; Fig. 11) showed relatively high DIC concentrations in the top 100 m on the shelf. Dissolved NH_4^+ was generally low ($< 1 \mu\text{mol L}^{-1}$) with small sub-surface (25–50 mbss) peaks of 2–3 $\mu\text{mol L}^{-1}$ at several OMZ and shelf stations. Furthermore, there was a marked bottom-water NH_4^+ accumulation up to 10 $\mu\text{mol L}^{-1}$ at station 6. At this station, a strong enrichment in NO_2^- was observed in the waters above the deep NH_4^+ peak. For the rest, NO_2^- concentrations were $< 1 \mu\text{mol L}^{-1}$ with small sub-surface peaks coinciding with peaks in NH_4^+ . Generally, the NO_3^- profiles showed surface-water depletion and downward increases to 30–40 $\mu\text{mol L}^{-1}$. Notable exception was the NO_3^- -depleted bottom water at station 6, where NO_3^- decreased from 25 to 0.3 $\mu\text{mol L}^{-1}$ between 50 and 100 mbss. The HPO_4^{2-} profiles generally showed down-ward increasing concentrations that stabilized at 2–3 $\mu\text{mol L}^{-1}$. Station 6 showed an increase in HPO_4^{2-} in the bottom 25 m to 4 $\mu\text{mol L}^{-1}$, concurring with the NH_4^+ peak. The molar DIN:DIP ratio, $(NH_4^+ + NO_2^- + NO_3^-) / HPO_4^{2-}$, was close to Redfield (14–16) throughout the water column at the slope and OMZ stations, except for lower ratios down to 6 in surface waters. At the shelf stations, by contrast, the DIN:DIP ratio was much more variable and showed decreases both in surface and bottom waters, most prominently at station 6 where the ratio declined to 3–4. Dissolved silica profiles showed down-ward increases up to 50 $\mu\text{mol L}^{-1}$, with relatively sharp

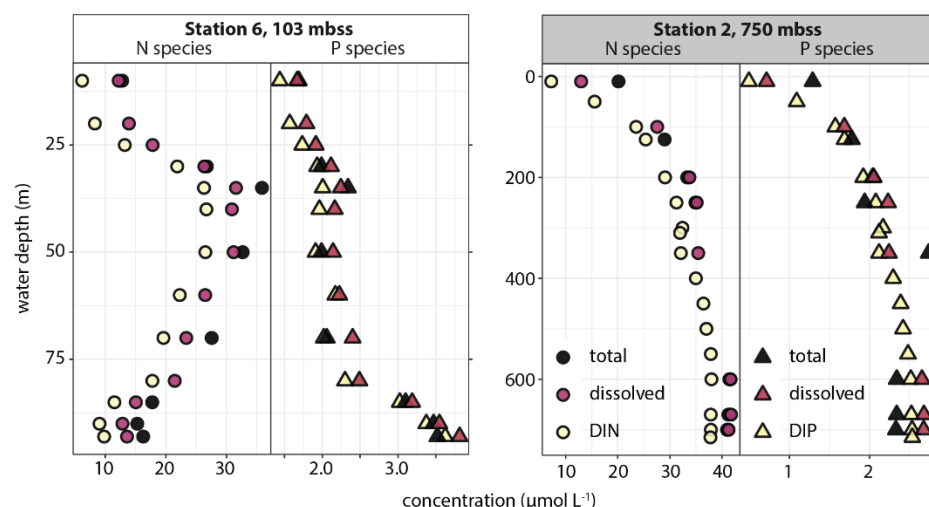


Figure 12: Water-column profiles of total, total dissolved and total dissolved inorganic N and P.

425

increases in deeper waters on the shelf. Also notable was the decline below 1250 mbss at Station 1, co-occurring with an increase in salinity (Fig. 11).

The measurement of various N and P species in selected water-column samples from stations 2 and 6 suggested small DON (3–6 $\mu\text{mol L}^{-1}$) and DOP (0.1–0.4 $\mu\text{mol L}^{-1}$) pools (Fig. 12). Furthermore, the difference between total N and total dissolved N in the deeper waters at station 6 (where turbidity was high; Fig. 10) suggested a particulate N pool that was roughly the same size as the DON pool. There was no evidence in the data for a particulate P pool.

430

4. Discussion

4.1. Sedimentary phosphorus pools: abundant highly reactive P on the shelf

435

Dissolved HPO_4^{2-} concentrations in the shelf sediment (stations 3, 4, 5, 6, 10) were about an order of magnitude higher than on the slope, reaching values up to 600 $\mu\text{mol L}^{-1}$ (Fig. 5). The pore-water profiles indicate differences in dominant P cycling processes between surficial and deeper sediment (Fig. 7). In the upper 10 cm of, measured pore-water HPO_4^{2-} concentrations were generally higher than calculated concentrations based on release of NH_4^+ and HPO_4^{2-} in Redfield stoichiometry of 16/1, except at station 3. Conversely, below 10 cm sediment depth, dissolved HPO_4^{2-} decreases strongly to concentrations that are well below calculated concentrations. These pore-water trends indicate (i) the presence of labile P pools other than OM that supply excess dissolved HPO_4^{2-} in the uppermost sediment and (ii) at depth, a process of sink-switching as the dissolved HPO_4^{2-} supply drives supersaturation and authigenic P precipitation, resulting in a strong decrease in pore-water HPO_4^{2-} (Ruttenberg, 1990; Anderson et al., 2001). These P cycling processes play a key role in regulating benthic exchange and P bioavailability; they result in strong gradients and fluxes around the sediment-water interface as well as long-term removal

440



of P by sink switching. Below, we use our and previous data to shed light on both the source of pore-water HPO_4^{2-} and likely
445 sinks.

Excess accumulation of HPO_4^{2-} relative to NH_4^+ in surficial sediment is often linked to reductive dissolution of Fe(III) (oxyhydr)oxides and release of sorbed P (Ruttenberg et al., 2003). However, the pool of Fe(III) (oxyhydr)oxides (FeOx) and associated P in sediments of the investigated BUS shelf stations is too small. These sediments are characterized by low contents of bulk solid-phase Fe and reactive FeOx: bulk Fe is generally $< 200 \mu\text{mol g}^{-1}$ ($\sim 1 \text{ wt.}\%$; except at depth in station 6
450 sediment) and almost all Fe is present as poorly and unreactive Fe, probably Fe in clays. The FeOx pool, estimated as the sum of HCl-Fe(III) and CDB-Fe, is $< 20 \mu\text{mol g}^{-1}$ (Fig. 4). The limited availability of reducible solid-phase Fe is further expressed in the low dissolved Fe^{2+} concentrations of at most $30 \mu\text{mol L}^{-1}$ (Fig. 5). Assuming a Fe/P stoichiometry of 5–10 for highly reactive Fe(III) (oxyhydr)oxides with sorbed or coprecipitated P (Jensen et al., 1992; Dzombak and Morel, 1990; Kraal et al., 2019), dissolution of reactive Fe and associated P would result in only a few $\mu\text{mol P L}^{-1}$. We conclude that
455 reductive Fe(III) dissolution is not a significant source of pore-water HPO_4^{2-} , explaining an insignificant fraction of the excess release of P amounting to $200\text{--}400 \mu\text{mol L}^{-1}$ (Fig. 7).

In upwelling areas such as the BUS but also the Arabian Sea and Peruvian upwelling system, high primary production supports large fish populations and associated fluxes of organic and mineral fish remains to the seafloor (Froelich et al., 1988; Schenau and De Lange, 2000; Suess, 1981). Fish bone consists for $\sim 50 \text{ wt.}\%$ of hydroxyapatite (HAP), a poorly
460 crystalline Ca-P mineral with the general formula $\text{Ca}_{10}(\text{PO}_4)_6(\text{OH})_2$ (Nriagu, 1982). This HAP is relatively efficiently buried in sediments underlying high-productivity waters, through a combination of high sedimentation rates and low oxygen availability which slows down microbial degradation processes. Our results indicate an important contribution of P-rich fish debris to the solid-phase P pool, firstly reflected in the low molar TOC/P ratios in the investigated shelf sediments (Fig. 3). In the surface sediment, dissolution of HAP in fish debris can be an important source of pore-water HPO_4^{2-} (Suess, 1981). In
465 an alternative process of sink switching, this additional accumulation of pore-water HPO_4^{2-} then drives authigenic precipitation of more stable carbonate fluorapatite (CFA), $\text{Ca}_{10}(\text{CO}_3, \text{PO}_4)_6\text{F}_2$ (Froelich et al., 1988; Schenau et al., 2000; Oxmann and Schwendenmann, 2015). Indeed, the decreases in pore-water F^- measured at several shelf stations (6, 10, 4) indicate active authigenic Ca-P formation at shelf stations (Fig. 5). In addition to direct precipitation of CFA, pore-water HPO_4^{2-} can be adsorbed onto CaCO_3 which is abundant in shelf sediments (Fig. 2). Over time, labile CaCO_3 -P converts into
470 more stable, crystalline Ca-P phases (Kraal et al., 2017; Manheim et al., 1975).

The results of sequential chemical P fractionation allow us to further explore the nature of solid-phase P. The high relative abundance of ex-P, Fe-P and Ca-P in the shelf sediments investigated in this study (Fig. 4), together accounting for $> 90\%$ of total solid-phase P, reflects the predominance of labile P pools that can easily transform and thereby drive intense P cycling. Here, we note that P adsorbed onto CaCO_3 can be misconstrued as Fe-associated P because the extractant targeting Fe-P also
475 dissolves CaCO_3 -associated P (Kraal et al., 2017). Overall, the sequential P extraction results should be treated with caution because of the uncertainty associated with using an operational chemical method to distinguish between labile P sources and sinks that likely represent a stability continuum (Oxmann and Schwendenmann, 2014; Kraal et al., 2017; Anderson and



Delaney, 2000). Sediments from the two stations with the highest and most variable P content (stations 6 and 10) contained visible, mm- to cm-scale fish debris (large fragments were removed prior to chemical analyses). The heterogeneous distribution of fish debris in the sediment likely resulted in the marked peaks in sediment P content and the relatively large discrepancy between total P from total digest and the sum of the sequentially extracted P pools (Fig. 2, 4). A chemical extraction method used to estimate the contribution of fish debris to the solid-phase P pool (Schenau and De Lange, 2000) indicated that HAP in fish bones constituted an important P pool (20 – 50% of total P in sediments on the continental slope (~1300 mbss) off Namibia in the BUS (Küster-Heins et al., 2010). If biogenic HAP was also present in slope sediment analysed in this study – station 2 at 750 mbss and station 7 at 1017 mbss, P extracted in the steps targeting Ca-P and Fe-P may in part be derived from biogenic HAP. We note that extraction of other labile Ca- and/or Fe-associated P by repeated NH_4Cl washes that target HAP could result in some overestimation of the biogenic HAP pool (Kraal et al., 2010b). In contrast to the apparent abundance of biogenic HAP as P pool in the BUS, a detailed study into P cycling on the Peruvian shelf and slope (74 – 1000 mbss) by Lomnitz et al. (2016) provided no evidence for an important role for fish debris as additional P source. These findings also contrast with previous work on the Peruvian shelf, which emphasized the central role of fish debris in the sedimentary P cycle and benthic P fluxes (Suess, 1981; Froelich et al., 1988). Rather than biogenic Ca-P, Lomnitz et al. (2016) highlighted the potential role of bacteria is supplying additional P to the sediment.

In addition to deposition of fish debris, P cycling in sediments from upwelling regions is known to be impacted by large sulphur-oxidizing bacteria (SOB) (Schulz and Schulz, 2005; Lomnitz et al., 2016; Cosmidis et al., 2013). Off Namibia, previous work has established the presence of SOB genera *Thiomargarita*, *Beggiatoa* and *Thioploca*, their presence and abundance varying in time and environmental conditions at the seafloor as bottom waters become seasonally anoxic and even sulfidic during late austral summer (Gallardo et al., 1998; Brüchert et al., 2003; Schulz and Schulz, 2005; Flood et al., 2021). Sulphur-oxidizing bacteria accumulate cellular P in the form of polyphosphates, releasing dissolved HPO_4^{2-} to the pore-water under reducing conditions and triggering formation of authigenic Ca-P and even phosphorite. The chemical P extraction procedure used here does not allow for quantification of polyphosphate-P, which could be extracted in the first few extraction steps as part of the labile P pool. We do note that exploratory analysis of sediment from station 6 with liquid-state (1 M NaOH extract) and solid-state ^{31}P -NMR did not reveal any indication of polyphosphate in the surface sediment (data not shown).

In the surface sediments from shelf stations 4, 5 and 6, we visually observed white filamentous microbes likely belonging to SOB genera (see Supplementary Information). Genetic analysis did not reveal the presence of SOB in surface (0 – 2 cm) sediment samples from stations 2 and 6 (data not shown), likely because of their low relative abundance compared to other microbial communities. Nonetheless, chemical signatures likely associated with SOB in the top sediment were observed in the pore-water profiles on the shelf, even at stations where there was no visual confirmation of SOB presence. At stations 3, 4, 5 and 10, dissolved HS^- accumulation only occurred at depth (> 5 cm) in the sediment (Fig. 5), while the sulphide oxidation product elemental sulphur was detected in the uppermost sediment < 5 cm (Fig. 3). Lastly, the top sediment was characterized by steep peaks in excess pore-water HPO_4^{2-} (Fig. 7) similar in shape and magnitude to those associated with



SOB in the work on the BUS shelf by Schulz and Schulz (Schulz and Schulz, 2005). In addition, unexpected peaks in pore-water NO_3^- and NO_2^- at depth in the reducing shelf sediment (Fig. 5) suggest the presence of SOB that concentrate NO_3^- in their vacuoles to use as electron acceptor for sulphide oxidation (Jørgensen and Gallardo, 1999; Schulz, 2006; Mchatton et al., 1996).

The SOB contribute to efficient reoxidation of HS^- produced by sulphate-reducing bacteria and drive rapid sulphur redox cycling in shelf sediments off Namibia (Dale et al., 2009). Furthermore, by inhibiting HS^- buildup in the uppermost sediment, SOB maintain weak HS^- gradients around the sediment-water interface and thereby limit benthic efflux of toxic HS^- (Ohde and Dadou, 2018; Flood et al., 2021). This despite the extremely high concentrations reached at relatively shallow depth (<20 cm) in the sediment; this study: 10 mmol L^{-1} and other studies: $> 20 \text{ mmol L}^{-1}$ (Brüchert et al., 2003). At the same time, steep pore-water HPO_4^{2-} gradients develop which result in high benthic HPO_4^{2-} fluxes, particularly at stations 5, 6 and 10. By contrast, shelf stations 3 and 4, with similar general sediment properties and environmental conditions (Table 3), showed a much smaller pool of excess HPO_4^{2-} (Fig. 7), much smaller labile P pools (Fig. 4) and relatively small P efflux (Fig. 8). These contrasting results for apparently similar shelf stations highlight that P cycling processes on the shelf in the BUS are highly variable not only temporally (seasonality of BWO and microbial communities) but also spatially, the latter perhaps revealing a high sensitivity of the P cycle to small differences in depositional conditions.

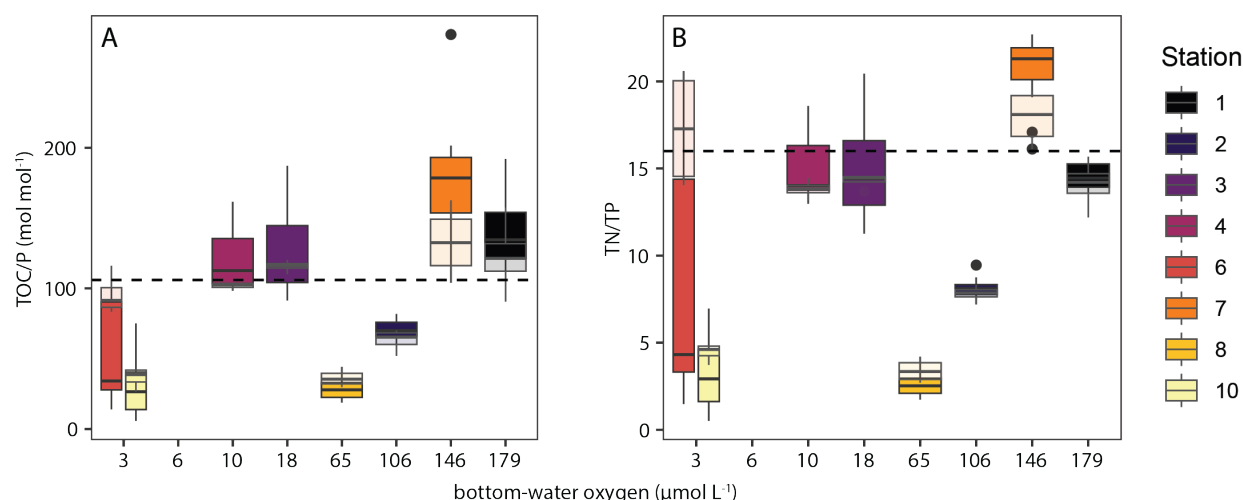
In summary, we find abundant pools of labile P in the BUS shelf sediments, which require an additional source of P as TOC/P ratios are very low. The available data suggest that HAP in fish debris may be an important, labile P source in this high-productivity area. Alternatively, or in addition, sulphur-oxidizing bacteria may introduce large amounts of P into the sediment and thereby trigger the formation of labile Ca-P phases. We propose that the stark difference in P abundance and speciation between shelf stations that have similar properties, i.e. large amounts of labile solid-phase P and excess HPO_4^{2-} at stations 5, 6 and 10 but not at stations 3 and 4, is suggestive of a dominant role for P supply by benthic bacteria that are highly sensitive to small temporal and spatial changes in depositional conditions. This seems more reasonable than highly localized deposition of fish debris onto sediment that is overlain by highly productive surface waters. The temporal and spatial variability in both the short-term (pore-water HPO_4^{2-} profiles, benthic fluxes) and long-term (solid-phase P profiles) aspects of the P cycle are significant. They indicate that (i) robust P budgets for upwelling systems can only be made with insight into seasonal variability and (ii) the functioning of the sediment as sink or source of P can change dramatically over time in response to even small changes in depositional conditions. Considering that upwelling systems are areas of (periodically) efficient and extensive P removal from the water column, the latter is a crucial consideration when forecasting the impact of environmental change (specifically deoxygenation) on the global marine P cycle.

4.2. Sediment C, N, P stoichiometry as function of depositional conditions

Ratios between TOC and (reactive) P are commonly used to reconstruct the redox conditions under which sediments have been deposited, with TOC/P ratios above the Redfield value (C:N:P in algal biomass $\approx 106:16:1$) indicative of increasingly strongly reducing conditions in the bottom water, where values > 400 are indicative of sulfidic bottom waters (Algeo and



545 Ingall, 2007; Kraal et al., 2010a; Kraal et al., 2012; Slomp et al., 2002). The foundation of this bottom-water redox proxy is work showing that oxygen depletion limits the P retention efficiency of the sediment and thereby increases the efficiency of P release from organic matter relative to C. Two processes play major roles: (i) the P retention capacity of bacteria diminishes under anaerobic conditions and (ii) the absence in reducing sediment of Fe (oxyhydr)oxides that can efficiently scavenge dissolved P (Ingall and Jahnke, 1994; Steenbergh et al., 2011; Mortimer, 1941; Gächter et al., 1988). Central in the relationship between TOC/P and bottom-water redox is the assumption that organic C and P are both delivered to the seafloor in algal biomass with approximately Redfield stoichiometry, 106:1 (Ruttenberg, 2014a). Therefore, interpretation of the sedimentary TOC/P ratio should consider other processes that may supply TOC and/or P with deviating C/P stoichiometry. This can be terrestrial organic matter with higher C/P than marine algal biomass (Ruttenberg and Goñi, 1997). Conversely, deposition or formation in the sediment of biogenic materials with relatively low C/P, such as (i) sulphur-oxidizing bacteria (SOB) with cellular polyphosphates and (ii) fish bones that contain several wt.% P with TOC/P ratios well below 100 (Wijayanti et al., 2021; Logesh et al., 2012; Løes et al., 2022), can decrease sedimentary TOC/P under oxygen-depleted bottom waters in productive marine regions and thereby affect the TOC/P–redox relationship.



560 **Figure 13: Molar TOC/P_{total} ratios (A) and (N/P)_{total} ratios (B) at selected stations along the investigated depth (redox) transect: box-and-whisker plots for data from top 15 cm (solid colours) and top 2 cm (“surface” sediment; semi-transparent colours). The lower and upper hinges correspond to the first and third quartiles (the 25th and 75th percentiles). The upper whisker extends from the hinge to the largest value no further than 1.5 * IQR from the hinge (where IQR is the inter-quartile range, or distance between the first and third quartiles). The lower whisker extends from the hinge to the smallest value at most 1.5 * IQR of the hinge. Data beyond the end of the whiskers are called "outlying" points and are plotted individually.**

Our results markedly deviate from a simple correlation between BWO and TOC/P (Fig. 13): the lowest TOC/P were recorded in shelf sediments underlying strongly oxygen depleted waters, while highest TOC/P values on the slope where bottom waters were reasonably well-oxygenated ($> 100 \mu\text{mol L}^{-1}$). Overall, we observe a reverse trend: TOC/P decreasing



570 with increasing oxygen depletion, indicating that the supply of additional P in SOB and fish debris can disrupt TOC/TP as
redox proxy in upwelling areas. While they did not explicitly address it, Lomnitz et al. (2016) did show additional P supply
(likely SOB) to the sediment other than sinking algal material in the Peruvian upwelling zone. By contrast, Kraal et al.
(2012) observed the more straightforward positive correlation between TOC/P and BWO along a redox gradient in the
Arabian Sea upwelling zone. In the latter study area, fish debris play an important role in benthic P cycling (Schenau and De
575 Lange, 2001) but pore-water sulphide accumulation is highly limited in surface sediments and therefore the Arabian Sea
sediments do not provide a suitable niche for SOB. This suggests that while biogenic P in fish debris can affect the TOC/TP
ratio, SOB may be predominantly responsible for actual disruption of the positive correlation between TOC/TP and BWO in
upwelling regions. As such, careful consideration of depositional conditions and P supply mechanisms is required when
interpreting TOC/P ratios in the context of redox conditions.

580 Regarding the role of SOB, it appears to make benthic P cycling and C, N, P stoichiometry highly sensitive to small changes
in environmental conditions. The four stations on the oxygen-depleted shelf ($BWO < 20 \mu\text{mol L}^{-1}$) show variable TOC/P
ratios from well below Redfield (stations 6 and 10; $BWO < 5 \mu\text{mol L}^{-1}$) to around Redfield (stations 3 and 4; $BWO 10\text{--}20$
 $\mu\text{mol L}^{-1}$). The strong difference in TOC/P within the narrow range of BWO on the shelf indicates that the role of SOB is
highly sensitive to redox conditions. Pore-water profiles showed sub-surface NO_3^- increases that suggest SOB-activity at all
585 shelf stations (Fig. 5). These peaks were slightly lower for stations 3 and 4 and here, excess HPO_4^{2-} was also relatively low
(Fig. 7). Furthermore, we observe that the N/P ratio mirrors the trend in TOC/P along the BWO transect (Fig. 13),
emphasizing that excess P supply and cycling rather than C dynamics control the TOC/P relationship.

Besides excess supply of P in biogenic Ca-P and by SOB, other factors also play a role in shaping TOC/P ratios, such as
shelf-to slope sediment transport and high biological activity and bioturbation in the OMZ. Station 7 (1027 MBSS) was
590 located in a ‘depo centre’ where OM, which has been resuspended from the shelf, is concentrated and buried (Inthorn et al.,
2006b; Inthorn et al., 2006a). Resuspended OM undergoes repetitive redox sequences and oxic respiration (Aller, 1998),
which selectively enriches C-rich compounds and thus enhances TOC/P. Contrasting with previous work that mentions the
refractory nature of OM in the depo centre, we note that relative high TOC content and benthic O_2 and DIC fluxes suggest
rapid breakdown of relatively fresh OM at station 7 during our visit. The peaks in turbidity in bottom waters observed at
595 most stations suggest active seafloor mass transport in a bottom nepheloid layer (Inthorn et al., 2006a) during our research
cruise (Fig. 10). In the OMZ, we observed abundant benthic faunal activity and burrows, suggesting active bioturbation and -
irrigation that can enhance OM breakdown in surface sediment by intensifying and prolonging exposure to high-energy-yield
oxidants such as O_2 and NO_3^- (Middelburg, 2018; Aller, 2014). In the sediment, this can lead to low TOC/P ratios (below
Redfield) as the C is lost as CO_2 or HCO_3^- while P is retained, likely by scavenging onto Fe (oxyhydr)oxides.

600 Overall, our results indicate that minor changes in environmental (redox) conditions in upwelling areas can strongly alter
benthic P burial mechanisms and efficiency. This is important because the extent, duration and intensity of oxygen depletion
in upwelling areas is changing as a result of anthropogenic global warming (Oschlies et al., 2018; Stramma et al., 2008;
Wright et al., 2012; Breitburg et al., 2018). Moreover, our results together with previous work suggest that large amounts of



P can be buried in strongly oxygen-depleted shelf environments of OMZs, because of (micro)biological processes such as P
605 accumulation by sulphur-oxidizing bacteria and by settling and burial of P-rich fish bones. Beyond the paradigm that marine
P burial efficiency decreases with decreasing BWO, distinct P deposition and cycling mechanisms in high-productivity areas
can introduce alternative, counteracting feedback mechanisms that disrupt the BWO–TOC/P relationship. With the majority
of global OM and P burial occurring on the shelf and slope in productive areas, such modulations of the redox dependence of
P burial can have marked implications for our understanding of P cycling and bioavailability under eutrophication and
610 intensifying ocean deoxygenation in the (ancient) past and the future.

4.3. Decoupled benthic nutrient fluxes and bottom-water chemistry

The calculated diffusive fluxes of the main oxidants for OM degradation (O_2 , NO_3^- , SO_4^{2-}) illustrate the transition from
anaerobic metabolism on the oxygen-depleted shelf to aerobic respiration on the slope (Fig. 8). On the shelf (stations 3, 4, 5,
6, 10), fluxes of NO_3^- and SO_4^{2-} into the sediment reflect denitrification and sulphate reduction. Beyond the shelf break
615 (stations 1, 2, 7, 8, 9), these fluxes decline and O_2 consumption is observed, indicating oxic respiration. The relatively low
consumption rate of O_2 on the slope compared to SO_4^{2-} on the shelf, together with a decrease in diffusive DIC release rates
with water depth, indicate that OM degradation rates are higher on the shelf where fresher OM is deposited at shallow water
depth and temperatures are higher (Fig. 10). The diffusive DIC fluxes on the shelf – and thus OM degradation rates – are
similar to those measured on the shelf in the Mauritanian upwelling system (Schroller-Lomnitz et al., 2019). The diffusive
620 SO_4^{2-} and DIC fluxes are highly variable on the shelf, reflecting heterogenous depositional conditions and sedimentary
environments. For shelf station 6, with strongly oxygen-depleted bottom waters and a surface sediment layer with strong
dissolved HS^- accumulation, we calculated a very high dissolved HS^- efflux from the sediment into the water column, two
orders of magnitude greater than nutrient fluxes. Periodically and locally extremely high benthic sulphide fluxes are a known
phenomenon in the NBUS and can result in sulphur plumes at the water surface that appear as light areas in ocean satellite
625 images (Ohde, 2018; Ohde and Dadou, 2018). No samples for dissolved HS^- fluxes were collected during whole-core
incubations.

The calculated benthic diffusive NH_4^+ and HPO_4^{2-} fluxes show that release of N and P from the sediment is highest from
organic-rich shelf sediments with low-oxygen bottom waters. The calculated diffusive HPO_4^{2-} fluxes on the shelf ($0.5\text{--}4$
 $\text{mmol m}^{-2} \text{d}^{-1}$) were in the same range as measured and calculated fluxes from the Arabian ($0.2\text{--}6 \text{mmol m}^{-2} \text{d}^{-1}$), Mauritanian
630 ($0.1\text{--}0.2 \text{mmol m}^{-2} \text{d}^{-1}$) and Peruvian ($0.2\text{--}1.5 \text{mmol m}^{-2} \text{d}^{-1}$) OMZs (Schenau and De Lange, 2001; Lomnitz et al., 2016;
Schroller-Lomnitz et al., 2019). The maximum measured HPO_4^{2-} release rate from the sediment at shelf station 4 ($\sim 1 \text{mmol}$
 $\text{m}^{-2} \text{d}^{-1}$) was similar to the maximum efflux measured under strongly oxygen-depleted bottom waters in the Peruvian OMZ
using in-situ sediment incubation chambers (Noffke et al., 2012). Our results show low values for the NH_4^+/HPO_4^{2-} ratio of
diffusive fluxes at most stations ($1\text{--}8 \text{mol mol}^{-1}$), well below the Redfield molar N/P ratio of 16, except at station 3
635 ($NH_4^+/HPO_4^{2-} = 19$). These low ratios result from high HPO_4^{2-} gradients around the sediment-water interface, driven by
excess release of HPO_4^{2-} relative to NH_4^+ (Fig. 8). As previously mentioned, we suggest that the excess HPO_4^{2-} accumulates



from dissolution of biogenic Ca-P and P release by SOB. Additionally, N released can be suppressed by anaerobic nitrogen-loss processes such as denitrification and anammox (Voss et al., 2013), which may constitute an efficient N sink in surface sediments where NO_3^- , NO_2^- and NH_4^+ co-occur in the absence of oxygen (Fig. 5). We found a strong correlation coefficient (Pearson's $r = 0.9$) between NH_4^+ and DIC diffusive fluxes, while the correlation coefficient between HPO_4^{2-} and DIC fluxes was much lower (Pearson's $r = 0.6$), further supporting a decoupling between OM degradation and sedimentary P effluxes (see Supplementary Information for the full correlation matrix).

While calculated diffusive and measured whole-core-incubation benthic fluxes of NH_4^+ and NO_3^- were similar in trend and magnitude, marked differences between calculations and measurements were observed for DIC and HPO_4^{2-} (Fig. 12). The DIC fluxes were up to two orders of magnitude higher than calculated fluxes and those measured in other upwelling areas, particularly at stations 6, 10 and 7. Furthermore, diffusive fluxes of total alkalinity were similar to diffusive DIC fluxes but measured TALK fluxes were one or two orders of magnitude lower (Fig. 8). These extremely high DIC fluxes seem robust as they were calculated based on linearly increasing DIC concentrations in the overlying water during triplicate core incubations (see Supplementary Information for incubation time series) but are difficult to explain. The observation that DIC fluxes far exceed TALK fluxes makes CaCO_3 dissolution unlikely, rather it suggests that CO_2 plays an important role in shaping the DIC flux. We note that stations 6 and 7, with the highest DIC fluxes, also show the strongest dissolved H_4SiO_4 enrichment in the bottom water; we propose that this may indicate a role for localized deposition and rapid degradation of sinking diatoms. Sediment chemistry and TOC content on the NBUS shelf is strongly impacted by the deposition of dead biomass from diatom blooms (Calvert and Price, 1983; Bremner, 1978; Borchers et al., 2005).

Regarding HPO_4^{2-} , the calculated and measured HPO_4^{2-} fluxes were in the same range but the trends between diffusive and net fluxes were very different. Rather: we calculated a decreasing trend in diffusive benthic efflux from the shelf to the slope but measured net HPO_4^{2-} fluxes on the shelf were high and highly variable, with positive (sediment to water) and negative (water to sediment) values. This variability is likely linked to spatially and temporally dynamic benthic P cycling processes. Deposition and breakdown of biogenic Ca-P as well as P sequestration and release by SOB can occur on short timescales, restricted to the uppermost sediment. Such processes cannot be adequately captured by cm-scale pore-water and sediment analysis. It also stresses that the overall role of NBUS sediments as sink or source of essential elements such as P can only be determined with long-term data of high temporal resolution, which is beyond the scope of this research expedition. The results from the diffusive calculations, whole-core flux measurements and bottom-water chemistry (more detail below) highlight that (i) benthic-pelagic coupling in the NBUS is not at steady state and (ii) benthic C, N and P fluxes become (temporarily) decoupled.

Evaluating bottom-water chemistry, we can further evaluate benthic-pelagic coupling and the impact of sediment biogeochemistry on water-column chemistry. This requires some caution, as pressure effects during coring can force pore-water into the overlying bottom water to an unknown extent. The results show chemical trends as function of surface-sediment OM enrichment and BWO (Fig. 9). Organic matter enrichment and BWO are strongly correlated (Pearson's $r = -0.72$; see Supplementary Information for correlation matrix), even though on the shelf TOC varies strongly within a narrow



range of BWO (Table 3). With decreasing BWO and increasing TOC, nutrient fluxes increase, and bottom waters become increasingly enriched in NH_4^+ , HPO_4^{2-} and H_4SiO_4 . The high Si concentration in bottom waters at slope station 7 may reflect dissolution of redeposited diatom frustules. While bottom-water nutrient concentrations generally increase with decreasing BWO and increasing sediment TOC enrichment, the bottom-water dissolved N/P ratio decreases strongly as these fluxes become decoupled. Furthermore, anaerobic N loss by denitrification is reflected in a strong decrease in bottom-water NO_3^- with decreasing BWO. Together with nutrients, dissolved HS^- also accumulated in the bottom waters at stations with oxygen-depleted bottom waters, most notably stations 6 and 10 for which positive diffusive HS^- fluxes were calculated (Fig. 12). The calculated fluxes for the latter stations varied strongly, while bottom-water HS^- concentrations were similar, suggesting that the pore-water chemistry from which the fluxes were calculated is a snapshot that may not reflect benthic exchange on longer timescales. In general, we note that samples were taken during late austral summer (early February) during which seasonal anoxia develops on the NBUS shelf and thus HS^- efflux is most likely to occur. Massive sulphide escape is known to occur regularly in this region, even leading to surface-water sulphur plumes thousands of km^2 in extent (Ohde and Dadou, 2018). While the mechanisms behind the extremely high DIC fluxes at some stations (6, 7, 10; Fig. 8) remain unclear, these appear to have resulted in relatively high bottom-water DIC concentrations at station 6 and 10 (Fig. 5).

685 4.4. Benthic and pelagic nitrogen and phosphorus cycling: implications of altered nutrient ratios

In the BUS, water-column N/P stoichiometry is affected by excess P release from the sediment (Emeis et al., 2017; Bailey, 1987; Flohr et al., 2014). In the NBUS region studied here, oxygen depletion in the water column drives (i) pelagic anaerobic N loss processes and (ii) benthic P supply that together result in off-shelf transport of N-depleted waters (Flohr et al., 2014). These processes drive N/P ratios in the water column to low values, resulting in the so-called ‘N deficit’ determined on the shelf during our research expedition (Van Kemenade et al., 2022), calculated as the difference between measured DIN and expected DIN based on HPO_4^{2-} (DIP) and Redfield stoichiometry ($\text{N/P} = 16$). As such, the N deficit is an operational indicator of the extent to which the measured N/P drops below the Redfield value. Our results illustrate how interacting sedimentary and pelagic biogeochemical processes result in shelf waters with molar N/P as low as 2.6 in deep waters (station 6, 100 mbss, $\text{BWO} = 3 \mu\text{mol L}^{-1}$).

695 Here, we use our nutrient data to estimate the impact of excess P supply to bottom waters on the N deficit, which is commonly regarded as a measure of anaerobic N loss relative to P. The water-column HPO_4^{2-} profiles for shelf stations 5, 6 and 10 show enrichments in the bottom ~25 m of $2.6\text{--}3.6 \mu\text{mol L}^{-1}$ (Fig. 11). Stations 3 and 4 do not show this enrichment; HPO_4^{2-} reaches $\sim 2 \mu\text{mol L}^{-1}$. We assume that this would have been the concentration of HPO_4^{2-} in bottom waters at stations 5, 6 and 10 as well in the hypothetical absence of the sediment-derived bottom-water HPO_4^{2-} enrichment. We can then calculate to what extent excess P (likely from sources other than algal OM; see section 4.1) rather than N depletion contributes to the calculated N deficit, the P-driven N deficit being the difference between the N deficit calculated with a deep-water P concentration of $2 \mu\text{mol L}^{-1}$ and the total N deficit ($\text{DIN} - 16 \times \text{DIP}$). The results are striking: 25–85% of the N



deficit can be contributed to the bottom-water excess P, likely delivered by the sediment (Fig. 14). This calls into question how accurate the term ‘N deficit’ is in the NBUS and perhaps more broadly in upwelling regions, as we show it can develop

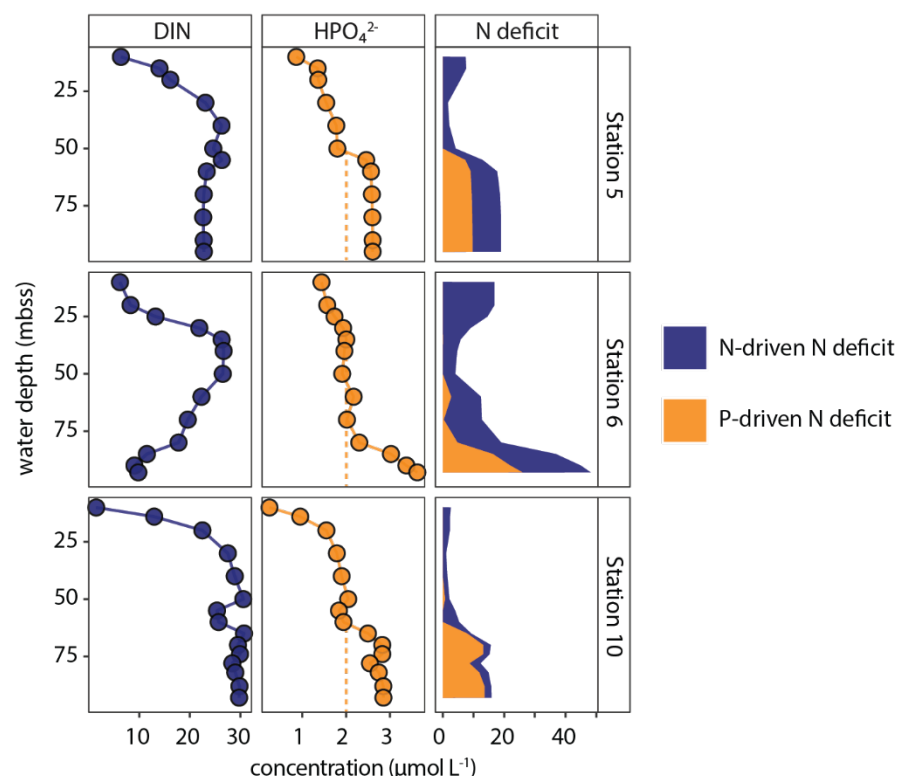


Figure 14: Water-column profiles of DIN (left panels) and HPO_4^{2-} (middle panels). Right panels show stacked plot of N deficit, showing the contributions from anaerobic N loss (blue) and excess supply of P (orange). The orange dashed lines show the ‘normal’ bottom-water HPO_4^{2-} concentrations that are assumed to represent P accumulation from algal OM breakdown; any additional P is considered excess P from other labile P sources (fish debris, sulphur-oxidizing bacteria) that contribute to the P-driven fraction of the N deficit.

without extensive anaerobic N loss (see station 10 in Fig. 14). Here, we do not consider in detail the processes underlying the N deficit calculated in surface waters, but we point out that a relative P excess is in line with global oceanic data showing that N commonly becomes depleted before P in the photic zone (Tyrrell, 1999).

Our results show dramatic changes in the dissolved N/P ratio in the waters on the oxygen-depleted NBUS shelf. Alteration of nutrient stoichiometry can have a profound impact on ocean biogeochemistry by affecting the microbial community composition (Moore et al., 2013). For instance, low N/P waters are thought to boost the relative abundance of N_2 -fixing cyanobacteria in both ancient (Kuypers et al., 2004) and modern marine systems including the NBUS (Emeis et al., 2017; Flohr et al., 2014; Vahtera et al., 2007). The physicochemical water-column data (temperature, density; Fig. 10) do not indicate strong stratification of the bottom waters, suggesting that the enrichment is due to active benthic P efflux and not bottom water restriction. However, our findings are in line with those of Flohr et al. (2014) in suggesting that the wider



impact of altered nutrient stoichiometry is minor, at least in the period the research cruise was undertaken. The water-column N/P ratios beyond the shelf break are close to Redfield throughout the water column; the waters transported off the shelf do not have a distinct, P-enriched and/or N-depleted signature. Our results do indicate that the increasing extent and intensity of ocean oxygen depletion in general and OMZs in particular have the potential to shift marine nutrient availability and stoichiometry through interacting, redox-dependent benthic and pelagic biogeochemical N and P cycling processes.

5. Conclusions

- High nutrient availability and strong redox gradients in the NBUS result in the formation and sediment burial of highly labile biogenic P phases such as calcium phosphate in fish bones and intracellular polyphosphate in sulphur-oxidizing bacteria on the oxygen-depleted shelf;
- The labile P pools have relatively low C/P and N/P ratios compared to algal OM (the predominant P source in most of the marine realm) and dissolve rapidly, leading to high concentrations of excess P in the pore-water and bottom water and thereby altering nutrient stoichiometry;
- Benthic P cycling and P fluxes on the oxygen-depleted shelf are highly variable in time and space with locally distinct depositional conditions and seasonal trends in bottom-water oxygenation; this complicates extrapolation of measurements for nutrient budgets;
- High fluxes of excess P from the sediment into the water column on the oxygen-depleted shelf locally affect water-column nutrient stoichiometry and contribute to the N deficit to the same extent as anaerobic microbial N loss, but this effect seems restricted to the shelf under current conditions;
- Ongoing ocean deoxygenation driven by eutrophication and global warming, specifically expansion and intensification of OMZs, will amplify changes in (de)coupled N-P cycling and stoichiometry and thereby impact ocean biogeochemistry and specifically the distribution of microbial communities.

Competing interests

The authors declare that they have no conflict of interest.

Author Contributions

PK led the research expedition, designed the on-board experiments and performed them together with KU, and wrote the manuscript with contributions from all co-authors. KU performed the on-board experiments and the on-shore laboratory analysis and contributed to the manuscript (review and editing). DR co-led the research expedition and contributed to the manuscript (review and editing). GJR contributed to the manuscript (review and editing).



750 Acknowledgements

We thank the crew, technical support and science party of Pelagia expedition 64PE449 to the northern Benguela upwelling system. Special thanks to Zeynep Erdem for the collaboration during cruise planning and execution. We are grateful to Karel Bakker for on-board nutrient analysis in water and pore-water samples. Royal NIOZ and National Marine facilities are thanked for financial support and providing ship time for this expedition. Laura Villanueva of NIOZ Marine Microbiology and Biogeochemistry performed DNA analysis in search of signatures of sulphur-oxidizing bacteria. Kasper Reitzel and Anna-Marie Klamt of the University of Southern Denmark (SDU) in Odense, Denmark, performed solid-state and liquid ^{31}P -NMR on sediment samples in search of polyphosphates. The work was financially supported under the UU–NIOZ agreement (2015–2025). Additional financial support for the research expedition was obtained from NIOZ.

References

- 760 Algeo, T. J. and Ingall, E.: Sedimentary $\text{C}_{\text{org}}:\text{P}$ ratios, paleocean ventilation, and Phanerozoic atmospheric pO_2 , *Palaeogeogr. Palaeoclimatol.*, 256, 130-155, doi:10.1016/j.palaeo.2007.02.029, 2007.
- Aller, R. C.: Mobile deltaic and continental shelf muds as suboxic, fluidized bed reactors, *Mar. Chem.*, 61, 143-155, 1998.
- Aller, R. C.: 8.11 - Sedimentary Diagenesis, Depositional Environments, and Benthic Fluxes, in: *Treatise on Geochemistry (Second Edition)*, edited by: Holland, H. D., and Turekian, K. K., Elsevier, Oxford, 293-334, <https://doi.org/10.1016/B978-0-08-095975-7.00611-2>, 2014.
- 765 Anderson, L. D. and Delaney, M. L.: Sequential extraction and analysis of phosphorus in marine sediments: Streamlining of the SEDEX procedure, *Limnol. Oceanogr.*, 45, 509-515, 2000.
- Anderson, L. D., Delaney, M. L., and Faul, K. L.: Carbon to phosphorus ratios in sediments: Implications for nutrient cycling, *Global Biogeochem. Cy.*, 15, 65-79, doi: 10.1029/2000gb001270, 2001.
- 770 Anschutz, P., Dedieu, K., Desmazes, F., and Chaillou, G.: Speciation, oxidation state, and reactivity of particulate manganese in marine sediments, *Chem. Geol.*, 218, 265-279, <https://doi.org/10.1016/j.chemgeo.2005.01.008>, 2005.
- APHA: Standard methods for the examination of water and wastewater, 21, American Public Health Association - American Water Works Association - Water Environment Federation 2005.
- Bailey, G. W.: The role of regeneration from the sediments in the supply of nutrients to the euphotic zone in the southern Benguela system, *South African Journal of Marine Science*, 5, 273-285, 10.2989/025776187784522478, 1987.
- 775 Bartlett, J. K. and Skoog, D. A.: Colorimetric determination of elemental sulfur in hydrocarbons, *Anal. Chem.*, 26, 1008-1011, 1954.
- Bograd, S. J., Jacox, M. G., Hazen, E. L., Lovecchio, E., Montes, I., Pozo Buil, M., Shannon, L. J., Sydeman, W. J., and Rykaczewski, R. R.: Climate Change Impacts on Eastern Boundary Upwelling Systems, *Annual Review of Marine Science*, 15, 303-328, <https://doi.org/10.1146/annurev-marine-032122-021945>, 2023.
- 780 Borchers, S. L., Schnetger, B., Böning, P., and Brumsack, H.-J.: Geochemical signatures of the Namibian diatom belt: Perennial upwelling and intermittent anoxia, *Geochem. Geophys. Geosyst.*, 6, doi:10.1029/2004GC000886, 2005.
- Breitbart, D., Levin, L. A., Oschlies, A., Grégoire, M., Chavez, F. P., Conley, D. J., Garçon, V., Gilbert, D., Gutiérrez, D., Isensee, K., Jacinto, G. S., Limburg, K. E., Montes, I., Naqvi, S. W. A., Pitcher, G. C., Rabalais, N. N., Roman, M. R., Rose, K. A., Seibel, B. A., Telszewski, M., Yasuhara, M., and Zhang, J.: Declining oxygen in the global ocean and coastal waters, *Science*, 359, 10.1126/science.aam7240, 2018.
- 785 Bremner, J. M.: Sediments on the continental margin off South West Africa between latitudes 17° and 25° S, 1978.
- Brüchert, V., Jørgensen, B. B., Neumann, K., Riechmann, D., Schlösser, M., and Schulz, H.: Regulation of bacterial sulfate reduction and hydrogen sulfide fluxes in the central namibian coastal upwelling zone, *Geochim. Cosmochim. Acta*, 67, 4505-4518, [https://doi.org/10.1016/S0016-7037\(03\)00275-8](https://doi.org/10.1016/S0016-7037(03)00275-8), 2003.
- 790



- Brüchert, V., Currie, B., Peard, K. R., Lass, U., Endler, R., Dübecke, A., Julies, E., Leipe, T., and Zitzmann, S.: BIOGEOCHEMICAL AND PHYSICAL CONTROL ON SHELF ANOXIA AND WATER COLUMN HYDROGEN SULPHIDE IN THE BENGUEL A COASTAL UPWELLING SYSTEM OFF NAMIBIA, Dordrecht, 161-193,
- Burdige, D. J.: Geochemistry of marine sediments, Princeton University Press 2006.
- 795 Burdige, D. J. and Komada, T.: Anaerobic oxidation of methane and the stoichiometry of remineralization processes in continental margin sediments, *Limnol. Oceanogr.*, 56, 1781-1796, <https://doi.org/10.4319/lo.2011.56.5.1781>, 2011.
- Burton, E. D., Sullivan, L. A., Bush, R. T., Johnston, S. G., and Keene, A. F.: A simple and inexpensive chromium-reducible sulfur method for acid-sulfate soils, *Appl. Geochem.*, 23, 2759-2766, 2008.
- Calvert, S. E. and Price, N. B.: Geochemistry of Namibian Shelf Sediments, in: Coastal Upwelling Its Sediment Record: Part A: Responses of the Sedimentary Regime to Present Coastal Upwelling, edited by: Suess, E., and Thiede, J., Springer US, Boston, MA, 337-375, 10.1007/978-1-4615-6651-9_17, 1983.
- 800 Chapman, P. and Shannon, L. V.: Seasonality in the oxygen minimum layers at the extremities of the Benguela system, *South African Journal of Marine Science*, 5, 85-94, 10.2989/025776187784522162, 1987.
- Chavez, F. P. and Messié, M.: A comparison of Eastern Boundary Upwelling Ecosystems, *Prog. Oceanogr.*, 83, 80-96, 805 <https://doi.org/10.1016/j.pocean.2009.07.032>, 2009.
- Claff, S. R., Sullivan, L. A., Burton, E. D., and Bush, R. T.: A sequential extraction procedure for acid sulfate soils: Partitioning of iron, *Geoderma*, 155, 224-230, 10.1016/j.geoderma.2009.12.002, 2010.
- Conley, D. J., Carstensen, J., Aigars, J., Axe, P., Bonsdorff, E., Eremina, T., Haahti, B.-M., Humborg, C., Jonsson, P., Kotta, J., Lännegren, C., Larsson, U., Maximov, A., Medina, M. R., Lysiak-Pastuszek, E., Remeikaitė-Nikienė, N., Walve, J., 810 Wilhelms, S., and Zillén, L.: Hypoxia Is Increasing in the Coastal Zone of the Baltic Sea, *Environ. Sci. Technol.*, 45, 6777-6783, 10.1021/es201212r, 2011.
- Cosmidis, J., Benzerara, K., Menguy, N., and Arning, E.: Microscopy evidence of bacterial microfossils in phosphorite crusts of the Peruvian shelf: implications for phosphogenesis mechanisms, *Chem. Geol.*, <http://dx.doi.org/10.1016/j.chemgeo.2013.09.009>, 2013.
- 815 Dale, A. W., Graco, M., and Wallmann, K.: Strong and Dynamic Benthic-Pelagic Coupling and Feedbacks in a Coastal Upwelling System (Peruvian Shelf), *Frontiers in Marine Science*, 4, 10.3389/fmars.2017.00029, 2017.
- Dale, A. W., Brüchert, V., Alperin, M., and Regnier, P.: An integrated sulfur isotope model for Namibian shelf sediments, *Geochim. Cosmochim. Acta*, 73, 1924-1944, <https://doi.org/10.1016/j.gca.2008.12.015>, 2009.
- Diaz, R. J. and Rosenberg, R.: Spreading dead zones and consequences for marine ecosystems, *Science*, 321, 926-929, 820 10.1126/science.1156401, 2008.
- Dzombak, D. A. and Morel, F. M. M.: Surface complexation modeling: Hydrous ferric oxide, Wiley, New York, 416 pp. 1990.
- Emeis, K., Eggert, A., Flohr, A., Lahajnar, N., Nausch, G., Neumann, A., Rixen, T., Schmidt, M., Van der Plas, A., and Wasmund, N.: Biogeochemical processes and turnover rates in the Northern Benguela Upwelling System, *J. Mar. Syst.*, 825 <https://doi.org/10.1016/j.jmarsys.2017.10.001>, 2017.
- Falkowski, P. G.: Evolution of the nitrogen cycle and its influence on the biological sequestration of CO₂ in the ocean, *Nature*, 387, 272-275, doi:10.1038/387272a0, 1997.
- Flohr, A., van der Plas, A. K., Emeis, K. C., Mohrholz, V., and Rixen, T.: Spatio-temporal patterns of C : N : P ratios in the northern Benguela upwelling system, *Biogeosciences*, 11, 885-897, 10.5194/bg-11-885-2014, 2014.
- 830 Flood, B. E., Louw, D. C., Van der Plas, A. K., and Bailey, J. V.: Giant sulfur bacteria (Beggiatoaceae) from sediments underlying the Benguela upwelling system host diverse microbiomes, *PLOS ONE*, 16, e0258124, 10.1371/journal.pone.0258124, 2021.
- Froelich, P. N., Arthur, M. A., Burnett, W. C., Deakin, M., Hensley, V., Jahnke, R., Kaul, L., Kim, K. H., Roe, K., Soutar, A., and Vathakanon, C.: Early diagenesis of organic-matter in Peru continental-margin sediments - Phosphorite precipitation, 835 *Mar. Geol.*, 80, 309-343, doi:10.1016/0025-3227(88)90095-3, 1988.
- Gächter, R., Meyer, J. S., and Mares, A.: Contribution of bacteria to release and fixation of phosphorus in lake-sediments, *Limnol. Oceanogr.*, 33, 1542-1558, 1988.
- Gallardo, V., Klingelhoeffer, E., Arntz, W., and Graco, M.: First report of the bacterium *Thioploca* in the Benguela ecosystem off Namibia, *Journal of the Marine Biological Association of the United Kingdom*, 78, 1007-1010, 1998.



- 840 Giraud, X., Le Quéré, C., and da Cunha, L. C.: Importance of coastal nutrient supply for global ocean biogeochemistry, *Global Biogeochem. Cy.*, 22, <https://doi.org/10.1029/2006GB002717>, 2008.
- Goldammer, T., Bruchert, V., Ferdelman, T. G., and Zabel, M.: Microbial sequestration of phosphorus in anoxic upwelling sediments, *Nature Geosci.*, 3, 557-561, doi:10.1038/ngeo913, 2010.
- Holland, H. D.: The chemistry of the atmosphere and oceans, Wiley, New York 1978.
- 845 Ingall, E. and Jahnke, R.: Evidence for enhanced phosphorus regeneration from marine sediments overlain by oxygen depleted waters, *Geochim. Cosmochim. Acta*, 58, 2571-2575, doi:10.1016/0016-7037(94)90033-7, 1994.
- Inthorn, M., Mohrholz, V., and Zabel, M.: Nepheloid layer distribution in the Benguela upwelling area offshore Namibia, *Deep-Sea Res. Pt. I*, 53, 1423-1438, 10.1016/j.dsr.2006.06.004, 2006a.
- Inthorn, M., Wagner, T., Scheeder, G., and Zabel, M.: Lateral transport controls distribution, quality, and burial of organic matter along continental slopes in high-productivity areas, *Geology*, 34, 205-208, 10.1130/G22153.1, 2006b.
- 850 Jenkyns, H. C.: Geochemistry of oceanic anoxic events, *Geochem. Geophys. Geosyst.*, 11, Q03004, 10.1029/2009gc002788, 2010.
- Jensen, H. S., Kristensen, P., Jeppesen, E., and Skytte, A.: Iron-phosphorus ratio in surface sediment as an indicator of phosphate release from aerobic sediments in shallow lakes, *Hydrobiologia*, 235, 731-743, 1992.
- 855 Jilbert, T., Jokinen, S., Saarinen, T., Mattus-Kumpunen, U., Simojoki, A., Saarni, S., Salminen, S., Niemistö, J., and Horppila, J.: Impacts of a deep reactive layer on sedimentary phosphorus dynamics in a boreal lake recovering from eutrophication, *Hydrobiologia*, 847, 4401-4423, 10.1007/s10750-020-04289-9, 2020.
- Jørgensen, B. B. and Gallardo, V. A.: *Thioploca* spp.: filamentous sulfur bacteria with nitrate vacuoles, *FEMS Microbiol. Ecol.*, 28, 301-313, 10.1111/j.1574-6941.1999.tb00585.x, 1999.
- 860 Kideys, A. E.: Fall and rise of the Black Sea ecosystem, *Science*, 297, 1482-1484, 2002.
- Kraal, P., Burton, E. D., and Bush, R. T.: Iron monosulfide accumulation and pyrite formation in eutrophic estuarine sediments, *Geochim. Cosmochim. Acta*, 122, 75-88, <http://dx.doi.org/10.1016/j.gca.2013.08.013>, 2013.
- Kraal, P., Slomp, C. P., and de Lange, G. J.: Sedimentary organic carbon to phosphorus ratios as a redox proxy in Quaternary records from the Mediterranean, *Chem. Geol.*, 277, 167-177, doi:10.1016/j.chemgeo.2010.08.003, 2010a.
- 865 Kraal, P., Dijkstra, N., Behrends, T., and Slomp, C. P.: Phosphorus burial in sediments of the sulfidic deep Black Sea: key roles for adsorption by calcium carbonate and apatite authigenesis, *Geochim. Cosmochim. Acta*, 204, 140-158, <http://dx.doi.org/10.1016/j.gca.2017.01.042>, 2017.
- Kraal, P., Slomp, C. P., Forster, A., and Kuypers, M. M. M.: Phosphorus cycling from the margin to abyssal depths in the proto-Atlantic during oceanic anoxic event 2, *Palaeogeogr. Palaeoclimatol.*, 295, 42-54, 2010b.
- 870 Kraal, P., van Genuchten, C. M., Behrends, T., and Rose, A. L.: Sorption of phosphate and silicate alters dissolution kinetics of poorly crystalline iron (oxyhydr)oxide, *Chemosphere*, 234, 690-701, 2019.
- Kraal, P., Slomp, C. P., Reed, D. C., Reichert, G. J., and Poulton, S. W.: Sedimentary phosphorus and iron cycling in and below the oxygen minimum zone of the northern Arabian Sea, *Biogeosciences*, 9, 2603-2624, 10.5194/bg-9-2603-2012, 2012.
- 875 Küster-Heins, K., Steinmetz, E., De Lange, G. J., and Zabel, M.: Phosphorus cycling in marine sediments from the continental margin off Namibia, *Mar. Geol.*, 274, 95-106, <https://doi.org/10.1016/j.margeo.2010.03.008>, 2010.
- Kuypers, M. M. M., van Breugel, Y., Schouten, S., Erba, E., and Sinninghe Damsté, J. S.: N₂-fixing cyanobacteria supplied nutrient N for Cretaceous oceanic anoxic events, *Geology*, 32, 853-856, 2004.
- Lenton, T. M. and Klausmeier, C. A.: Biotic stoichiometric controls on the deep ocean N : P ratio, *Biogeosciences*, 4, 353-367, 2007.
- 880 Løes, A.-K., Ahlin, J. P., Ahuja, I., Krogstad, T., Smevoll, S., and Waag, H.: Effects of Formic Acid Preservation of Fishbones on the Extractability of Ammonium Lactate–Acetate Soluble Calcium, Phosphorus, Magnesium, and Potassium, *Waste and Biomass Valorization*, 13, 3547-3559, 10.1007/s12649-022-01744-7, 2022.
- Logesh, A. R., Pravinkumar, M., Raffi, S. M., and Kalaiselvam, M.: Calcium and phosphorus determination in bones of low value fishes, *Sardinella longiceps* (Valenciennes) and *Trichiurus savala* (Cuvier), from Parangipettai, Southeast Coast of India, *Asian Pacific Journal of Tropical Disease*, 2, S254-S256, [https://doi.org/10.1016/S2222-1808\(12\)60160-1](https://doi.org/10.1016/S2222-1808(12)60160-1), 2012.
- 885 Lomnitz, U., Sommer, S., Dale, A. W., Löscher, C. R., Noffke, A., Wallmann, K., and Hensen, C.: Benthic phosphorus cycling in the Peruvian oxygen minimum zone, *Biogeosciences*, 13, 1367-1386, 10.5194/bg-13-1367-2016, 2016.



- Manheim, F., Rowe, G. T., and Jipa, D.: Marine phosphorite formation off Peru, *Journal of Sedimentary Research*, 45, 243-251, 10.1306/212f6d20-2b24-11d7-8648000102c1865d, 1975.
- Marcus, N. H. and Boero, F.: Minireview: The importance of benthic-pelagic coupling and the forgotten role of life cycles in coastal aquatic systems, *Limnol. Oceanogr.*, 43, 763-768, <https://doi.org/10.4319/lo.1998.43.5.0763>, 1998.
- McHatton, S. C., Barry, J. P., Jannasch, H. W., and Nelson, D. C.: High Nitrate Concentrations in Vacuolate, Autotrophic Marine Beggiatoa spp, *Appl. Environ. Microb.*, 62, 954-958, doi:10.1128/aem.62.3.954-958.1996, 1996.
- 895 Meier, H. E. M., Andersson, H. C., Eilola, K., Gustafsson, B. G., Kuznetsov, I., Müller-Karulis, B., Neumann, T., and Savchuk, O. P.: Hypoxia in future climates: A model ensemble study for the Baltic Sea, *Geophys. Res. Lett.*, 38, L24608, 10.1029/2011gl049929, 2011.
- Messié, M. and Chavez, F. P.: Seasonal regulation of primary production in eastern boundary upwelling systems, *Prog. Oceanogr.*, 134, 1-18, <https://doi.org/10.1016/j.pocean.2014.10.011>, 2015.
- 900 Middelburg, J. J.: Reviews and syntheses: to the bottom of carbon processing at the seafloor, *Biogeosciences*, 15, 413-427, 10.5194/bg-15-413-2018, 2018.
- Middelburg, J. J. and Levin, L. A.: Coastal hypoxia and sediment biogeochemistry, *Biogeosciences*, 6, 1273-1293, 10.5194/bg-6-1273-2009, 2009.
- Mohrholz, V., Bartholomae, C. H., van der Plas, A. K., and Lass, H. U.: The seasonal variability of the northern Benguela undercurrent and its relation to the oxygen budget on the shelf, *Cont. Shelf Res.*, 28, 424-441, <https://doi.org/10.1016/j.csr.2007.10.001>, 2008.
- Mohrholz, V., Eggert, A., Junker, T., Nausch, G., Ohde, T., and Schmidt, M.: Cross shelf hydrographic and hydrochemical conditions and their short term variability at the northern Benguela during a normal upwelling season, *J. Mar. Syst.*, 140, 92-110, <https://doi.org/10.1016/j.jmarsys.2014.04.019>, 2014.
- 910 Moore, C. M., Mills, M. M., Arrigo, K. R., Berman-Frank, I., Bopp, L., Boyd, P. W., Galbraith, E. D., Geider, R. J., Guieu, C., Jaccard, S. L., Jickells, T. D., La Roche, J., Lenton, T. M., Mahowald, N. M., Maranon, E., Marinov, I., Moore, J. K., Nakatsuka, T., Oschlies, A., Saito, M. A., Thingstad, T. F., Tsuda, A., and Ulloa, O.: Processes and patterns of oceanic nutrient limitation, *Nature Geosci.*, 6, 701-710, 10.1038/ngeo1765 <http://www.nature.com/ngeo/journal/v6/n9/abs/ngeo1765.html#supplementary-information>, 2013.
- 915 Moreno, A. R. and Martiny, A. C.: Ecological Stoichiometry of Ocean Plankton, *Annual Review of Marine Science*, 10, 43-69, 10.1146/annurev-marine-121916-063126, 2018.
- Mort, H. P., Adatte, T., Föllmi, K. B., Keller, G., Steinmann, P., Matera, V., Berner, Z., and Stüben, D.: Phosphorus and the roles of productivity and nutrient recycling during oceanic anoxic event 2, *Geology*, 35, 483-486, 2007.
- Mortimer, C. H.: The exchange of dissolved substances between mud and water, *Journal of Ecology*, 29, 280-329, 1941.
- 920 Nagel, B., Gaye, B., Lahajnar, N., Struck, U., and Emeis, K.-C.: Effects of current regimes and oxygenation on particulate matter preservation on the Namibian shelf: Insights from amino acid biogeochemistry, *Mar. Chem.*, 186, 121-132, <https://doi.org/10.1016/j.marchem.2016.09.001>, 2016.
- Nagel, B., Emeis, K. C., Flohr, A., Rixen, T., Schlarbaum, T., Mohrholz, V., and Plas, A.: N-cycling and balancing of the N-deficit generated in the oxygen minimum zone over the Namibian shelf—An isotope-based approach, *Journal of Geophysical Research: Biogeosciences*, 118, 361-371, doi:10.1002/jgrg.20040, 2013.
- 925 Needoba, J. A., Foster, R. A., Sakamoto, C., Zehr, J. P., and Johnson, K. S.: Nitrogen fixation by unicellular diazotrophic cyanobacteria in the temperate oligotrophic North Pacific Ocean, *Limnol. Oceanogr.*, 52, 1317-1327, <https://doi.org/10.4319/lo.2007.52.4.1317>, 2007.
- Noffke, A., Hensen, C., Sommer, S., Scholz, F., Bohlen, L., Mosch, T., Graco, M., and Wallmann, K.: Benthic iron and phosphorus fluxes across the Peruvian oxygen minimum zone, *Limnol. Oceanogr.*, 57, 851-867, <https://doi.org/10.4319/lo.2012.57.3.0851>, 2012.
- 930 Nriagu, J. O.: Rapid decomposition of fish bones in Lake Erie sediments, *Hydrobiologia*, 106, 217-222, 1982.
- Ohde, T.: Coastal Sulfur Plumes off Peru During El Niño, La Niña, and Neutral Phases, *Geophys. Res. Lett.*, 45, doi:10.1029/2018GL077618, 2018.
- 935 Ohde, T. and Dadou, I.: Seasonal and annual variability of coastal sulphur plumes in the northern Benguela upwelling system, *PLOS ONE*, 13, e0192140, 10.1371/journal.pone.0192140, 2018.
- Oschlies, A., Brandt, P., Stramma, L., and Schmidtko, S.: Drivers and mechanisms of ocean deoxygenation, *Nature Geosci.*, 11, 467-473, 10.1038/s41561-018-0152-2, 2018.



- 940 Oxmann, J. F. and Schwendenmann, L.: Quantification of octacalcium phosphate, authigenic apatite and detrital apatite in coastal sediments using differential dissolution and standard addition, *Ocean Sci.*, 10, 571-585, 10.5194/os-10-571-2014, 2014.
- Oxmann, J. F. and Schwendenmann, L.: Authigenic apatite and octacalcium phosphate formation due to adsorption–precipitation switching across estuarine salinity gradients, *Biogeosciences*, 12, 723-738, 10.5194/bg-12-723-2015, 2015.
- 945 Poulton, S. W. and Canfield, D. E.: Development of a sequential extraction procedure for iron: implications for iron partitioning in continentally derived particulates, *Chem. Geol.*, 214, 209-221, doi:10.1016/j.chemgeo.2004.09.003, 2005.
- Raven, J. A. and Falkowski, P. G.: Oceanic sinks for atmospheric CO₂, *Plant, Cell & Environment*, 22, 741-755, 10.1046/j.1365-3040.1999.00419.x, 1999.
- Redfield, A. C.: The biological control of chemical factors in the environment, *Am. Sci.*, 46, 205-222, 1958.
- 950 Reinhard, C. T., Planavsky, N. J., Gill, B. C., Ozaki, K., Robbins, L. J., Lyons, T. W., Fischer, W. W., Wang, C., Cole, D. B., and Konhauser, K. O.: Evolution of the global phosphorus cycle, *Nature*, 541, 386-389, 10.1038/nature20772, 2017.
- Ruttenberg, K. C.: Diagenesis and burial of phosphorus in marine sediments : implications for the marine phosphorus budget, Yale University, New Haven, 375 pp., 1990.
- Ruttenberg, K. C.: Development of a sequential extraction method for different forms of phosphorus in marine sediments, *Limnol. Oceanogr.*, 37, 1460-1482, 1992.
- 955 Ruttenberg, K. C.: Reassessment of the oceanic residence time of phosphorus, *Chem. Geol.*, 107, 405-409, 1993.
- Ruttenberg, K. C.: The Global Phosphorus Cycle, in: *Treatise on Geochemistry (Second Edition)*, edited by: Holland, H. D., and Turekian, K. K., Elsevier, Oxford, 499-558, <https://doi.org/10.1016/B978-0-08-095975-7.00813-5>, 2014a.
- Ruttenberg, K. C.: 10.13 - The Global Phosphorus Cycle, in: *Treatise on Geochemistry (Second Edition)*, edited by: Holland, H. D., and Turekian, K. K., Elsevier, Oxford, 499-558, <https://doi.org/10.1016/B978-0-08-095975-7.00813-5>, 2014b.
- 960 Ruttenberg, K. C. and Goñi, M. A.: Phosphorus distribution, C:N:P ratios, and $\delta^{13}\text{C}_{\text{org}}$ in arctic, temperate, and tropical coastal sediments: tools for characterizing bulk sedimentary organic matter, *Mar. Geol.*, 139, 123-145, [https://doi.org/10.1016/S0025-3227\(96\)00107-7](https://doi.org/10.1016/S0025-3227(96)00107-7), 1997.
- Ruttenberg, K. C., Holland, H. D., and Turekian, K. K.: The global phosphorus cycle, in: *Treatise on Geochemistry*, edited by: Schlesinger, W. H., Pergamon, Oxford, 585-643, 2003.
- 965 Schenau, S. J. and De Lange, G. J.: A novel chemical method to quantify fish debris in marine sediments, *Limnol. Oceanogr.*, 45, 963-971, 2000.
- Schenau, S. J. and De Lange, G. J.: Phosphorus regeneration vs. burial in sediments of the Arabian Sea, *Mar. Chem.*, 75, 201-217, doi:10.1016/S0304-4203(01)00037-8, 2001.
- Schenau, S. J., Slomp, C. P., and De Lange, G. J.: Phosphogenesis and active phosphorite formation in sediments from the 970 Arabian Sea oxygen minimum zone, *Mar. Geol.*, 169, 1-20, doi:10.1016/S0025-3227(00)00083-9, 2000.
- Schroller-Lomnitz, U., Hensen, C., Dale, A. W., Scholz, F., Clemens, D., Sommer, S., Noffke, A., and Wallmann, K.: Dissolved benthic phosphate, iron and carbon fluxes in the Mauritanian upwelling system and implications for ongoing deoxygenation, *Deep Sea Res. Pt. 1*, 143, 70-84, <https://doi.org/10.1016/j.dsr.2018.11.008>, 2019.
- Schulz, H. N.: The genus *Thiomargarita*, *Prokaryotes*, 6, 1156-1163, 2006.
- 975 Schulz, H. N. and Schulz, H. D.: Large sulfur bacteria and the formation of phosphorite, *Science*, 307, 416-418, 2005.
- Shannon, L. V., Agenbag, J. J., and Buys, M. E. L.: Large- and mesoscale features of the Angola-Benguela front, *South African Journal of Marine Science*, 5, 11-34, 10.2989/025776187784522261, 1987.
- Slomp, C. P., Thomson, J., and De Lange, G. J.: Enhanced regeneration of phosphorus during formation of the most recent eastern Mediterranean sapropel (S1), *Geochim. Cosmochim. Acta*, 66, 1171-1184, doi:10.1016/S0016-7037(01)00848-1, 2002.
- 980 Slomp, C. P., Thomson, J., and De Lange, G. J.: Controls on phosphorus regeneration and burial during formation of eastern Mediterranean sapropels, *Mar. Geol.*, 203, 141-159, 2004.
- Steenbergh, A. K., Bodelier, P. L. E., Hoogveld, H. L., Slomp, C. P., and Laanbroek, H. J.: Phosphatases relieve carbon limitation of microbial activity in Baltic Sea sediments along a redox-gradient, *Limnol. Oceanogr.*, 56, 2018-2026, doi:10.4319/lo.2011.56.6.2018, 2011.
- Stramma, L., Johnson, G. C., Sprintall, J., and Mohrholz, V.: Expanding oxygen-minimum zones in the tropical oceans, *Science*, 320, 655-658, 10.1126/science.1153847, 2008.



- Stüeken, E. E., Kipp, M. A., Koehler, M. C., and Buick, R.: The evolution of Earth's biogeochemical nitrogen cycle, *Earth-Sci. Rev.*, 160, 220-239, <https://doi.org/10.1016/j.earscirev.2016.07.007>, 2016.
- 990 Suess, E.: Phosphate regeneration from sediments of the Peru continental margin by dissolution of fish debris, *Geochim. Cosmochim. Acta*, 45, 577-588, doi:10.1016/0016-7037(81)90191-5, 1981.
- Summerhayes, C. P., Kroon, D., Rosell-Melé, A., Jordan, R. W., Schrader, H. J., Hearn, R., Villanueva, J., Grimalt, J. O., and Eglinton, G.: Variability in the Benguela Current upwelling system over the past 70,000 years, *Prog. Oceanogr.*, 35, 207-251, [https://doi.org/10.1016/0079-6611\(95\)00008-5](https://doi.org/10.1016/0079-6611(95)00008-5), 1995.
- 995 Tyrrell, T.: The relative influences of nitrogen and phosphorus on oceanic primary production, *Nature*, 400, 525-531, doi:10.1038/22941, 1999.
- Vahtera, E., Conley, D. J., Gustafsson, B. G., Kuosa, H., Pitkänen, H., Savchuk, O. P., Tamminen, T., Viitasalo, M., Voss, M., Wasmund, N., and Wulff, F.: Internal Ecosystem Feedbacks Enhance Nitrogen-fixing Cyanobacteria Blooms and Complicate Management in the Baltic Sea, *AMBIO: A Journal of the Human Environment*, 36, 186-194, 189, 2007.
- 1000 van Kemenade, Z. R., Villanueva, L., Hopmans, E. C., Kraal, P., Witte, H. J., Sinninghe Damsté, J. S., and Rush, D.: Bacteriohopanetetrol-x: constraining its application as a lipid biomarker for marine anammox using the water column oxygen gradient of the Benguela upwelling system, *Biogeosciences*, 19, 201-221, 10.5194/bg-19-201-2022, 2022.
- Voss, M., Bange, H. W., Dippner, J. W., Middelburg, J. J., Montoya, J. P., and Ward, B.: The marine nitrogen cycle: recent discoveries, uncertainties and the potential relevance of climate change, *Philosophical Transactions of the Royal Society B: Biological Sciences*, 368, 10.1098/rstb.2013.0121, 2013.
- 1005 Wijayanti, I., Benjakul, S., and Sookchoo, P.: Effect of high pressure heating on physical and chemical characteristics of Asian sea bass (*Lates calcarifer*) backbone, *Journal of food science and technology*, 58, 3120-3129, 10.1007/s13197-020-04815-6, 2021.
- 1010 Wright, J. J., Konwar, K. M., and Hallam, S. J.: Microbial ecology of expanding oxygen minimum zones, *Nat. Rev. Microbiol.*, 10, 381-394, 10.1038/nrmicro2778, 2012.